JGR Atmospheres

RESEARCH ARTICLE
10.1029/2018JD029681

Special Section:
3D Cloud Modeling as a Tool for 3D Radiative Transfer

An Assessment of the Impacts of Cloud Vertical Heterogeneity on Global Ice Cloud Data Records From Passive Satellite Retrievals

Chenxi Wang[1,2], Steven Platnick[2], Thomas Fauchez[3,2], Kerry Meyer[2], Zhibo Zhang[4], Hironobu Iwabuchi[5], and Brian H. Kahn[6]

[1]Earth System Science Interdisciplinary Center, University of Maryland College Park, College Park, MD, USA, [2]NASA Goddard Space Flight Center, Greenbelt, MD, USA, [3]Universities Space Research Association, Columbia, MD, USA, [4]Department of Physics, University of Maryland Baltimore County, Baltimore, MD, USA, [5]Center for Atmospheric and Oceanic Studies, Graduate School of Science, Tohoku University, Sendai, Japan, [6]Jet Propulsion Laboratory, California Institute of Technology, Pasadena, CA, USA

Abstract Spaceborne passive instruments are widely used to infer long-term ice cloud properties due to their large temporal and spatial coverage. Although observations from active instruments demonstrate ice particle variability in the vertical dimension, a pragmatic assumption made in passive cloud retrieval algorithms is that the observed scene consists of a plane-parallel cloud. In this study, a theoretical exploration on how ice cloud vertical heterogeneity (ICVH) influences passive retrievals (i.e., cloud optical thickness, cloud effective radius, and ice water path, IWP) is implemented at the pixel scale. Specifically, with an established ice cloud profile database inferred from 1-year Cloud-Aerosol Lidar and Infrared Pathfinder Satellite Observation/CloudSat, we quantitatively estimate ICVH-induced biases on monthly averaged cloud macrophysical and radiative properties. Results show an average underestimation (−35%) of Moderate Resolution Imaging Spectroradiometer (MODIS) monthly IWP due to the ICVH for global ice clouds over ocean. The ICVH impacts are enhanced at large IWPs (e.g., > 500 g/m^2) and solar zenith angles, resulting in a profound underestimation of MODIS IWP (up to −50%) in deep convective regions and middle to high-latitude regions in the winter hemisphere. The global-averaged ice cloudy-sky reflected solar radiation and outgoing longwave radiation derived from MODIS retrievals are slightly overestimated, suggesting that the ICVH has little impact on cloud radiative properties. Relatively large reflected solar radiation (0.3 W/m^2) and outgoing longwave radiation (0.1 W/m^2) flux differences occur at high and low IWPs, respectively. The largest total flux difference (~2 W/m^2), mainly contributed by shortwave part, is associated with deep convection where the typical IWP is greater than 2,000 g/m^2.

Key Points:
- Derived IWP based on the plane-parallel approximation can be underestimated by more than 50% due to ice cloud vertical heterogeneity
- ICVH has little impact on flux calculations as long as the same assumptions are made in both the calculations and the cloud retrievals
- IWP differences between the MODIS-like and active sensor-based retrievals can be partly explained by ice cloud vertical heterogeneity

Supporting Information:
- Supporting Information S1
- Figure S1
- Figure S2
- Figure S3

Correspondence to:
C. Wang,
chenxi.wang@nasa.gov

Citation:
Wang, C., Platnick, S., Fauchez, T., Meyer, K., Zhang, Z., Iwabuchi, H., & Kahn, B. H. (2019). An assessment of the impacts of cloud vertical heterogeneity on global ice cloud data records from passive satellite retrievals. *Journal of Geophysical Research: Atmospheres*, *124*, 1578–1595. https://doi.org/10.1029/2018JD029681

Received 21 SEP 2018
Accepted 20 DEC 2018
Accepted article online 26 DEC 2018
Published online 2 FEB 2019

1. Introduction

Ice clouds have long been viewed as one of the most important components of the climate system because of their substantial impacts on the Earth's radiation balance (Stephens et al., 2012; Trenberth et al., 2009) and global hydrologic cycle (Chahine, 1992; Mülmenstädt et al., 2015; Stubenrauch et al., 2013). Tremendous efforts have been made to reproduce ice cloud processes in models; however, the representation of ice cloud microphysical and macrophysical properties in current climate models remains one of the largest sources of uncertainty in predicting climate variability and changes (Boucher et al., 2013; Houghton et al., 2001; Randall et al., 2007; Su et al., 2013). Previous studies have shown that the globally averaged annual mean ice water path (IWP) from the models differ by more than 1 order of magnitude (Eliasson et al., 2011; Jiang et al., 2012; Taylor et al., 2012; Waliser et al., 2009), which is much larger than other modeled atmospheric variables. Meanwhile, parallel efforts focused on cloud in situ measurements and remote sensing techniques have been undertaken to understand cloud optical and microphysical properties (Baumgardner et al., 2017; Deng et al., 2015; Ferraro et al., 2005; Platnick et al., 2017; Rossow & Schiffer, 1999), to improve cloud parameterization schemes in models (Fu & Liou, 1993; Morrison & Mibrandt, 2015), and to provide observational constraints on model evaluations (Stubenrauch et al., 2013; Su et al., 2013; Vogelmann & Ackerman, 1995). Among a large variety of observations, satellite-based products provide the most continuous and comprehensive records for global ice clouds. However, comparison of ice cloud properties from different satellite instruments suggests a considerable diversity (Duncan & Eriksson, 2018; Eliasson et al., 2011; Eriksson et al., 2008; Horváth & Davies, 2007; Stubenrauch et al.,

2013; Wu et al., 2009), though typically not as large in magnitude as intermodel differences (e.g., Waliser et al., 2009), making it more difficult to evaluate climate models (Waliser et al., 2007). Understanding and decreasing interobservation diversity is therefore a critical component for reducing uncertainties in climate prediction.

Observational discrepancies of ice clouds among various satellite instruments can be largely attributed to information content differences among different instruments (Stephens & Kummerow, 2007; Wu et al., 2009), oversimplified ice particle microphysical models (Yang et al., 2013) and forward radiative transfer models (Fauchez et al., 2015, 2018). Actually, ice cloud properties retrieved from individual instruments suffer from inevitable limitations that are determined by instrument types (e.g., passive or active sensors) and selected spectral channels. For example, a typical active spaceborne lidar has an upper limit of ice cloud visible optical thickness ~3 before signals at 532 nm from underlying cloud layers are completely attenuated. Passive shortwave (SW) and microwave instruments, however, can detect radiation from optically deeper cloud layers. For example, the current version (C6.1) of MODIS has an upper limit of IWP around 5.5 kg/m^2, and microwave instruments (at 157 and 183 GHz) have higher limits up to 10 kg/m^2 (Gong & Wu, 2014; Holl et al., 2014). A joint retrieval algorithm that utilizes channels from different instruments is an effective approach to overcome the limited information content of an individual instrument (Holl et al., 2014; Sourdeval et al., 2013). Cloud retrieval error sources also include forward model assumptions. For example, a common assumption made in prevailing passive cloud remote sensing techniques is the Plane-Parallel Homogeneous (PPH) approximation (Chang et al., 2017; Garnier et al., 2012, 2013; Heidinger et al., 2014; Platnick et al., 2017; Wang et al., 2011; Wang, Platnick, Zhang, Meyer, & Yang, 2016; Wang, Platnick, Zhang, Meyer, Wind, et al., 2016), which assumes that clouds are horizontally and vertically homogeneous. A less restrictive Independent Pixel Approximation (IPA) can capture cloud particle variations in the vertical direction. The IPA assumption prohibits radiation transfer from one column (pixel) to contiguous columns (pixels), allowing the use of a 1D radiative transfer model in the cloud retrieval algorithm. Studies showing that pixel-level cloud retrievals may be biased using the PPH and/or IPA assumptions have been reported for liquid water clouds (e.g., Marshak et al., 2006; Platnick, 2000; Várnai & Davies, 1999; Zhang et al., 2012, 2016) and for ice clouds (Fauchez, Davis, et al., 2017; Fauchez, Platnick, et al., 2017). These pixel-level retrieval biases may impact studies relying on satellite climate records (e.g., Level-3 aggregated cloud products). Numerous works have quantitatively estimated the impacts from various cloud heterogeneities, namely, vertical heterogeneity (Platnick, 2000; van Diedenhoven et al., 2016; Zhang et al., 2012), horizontal and subpixel heterogeneity (Fauchez et al., 2015; Kahn et al., 2015; Zhang et al., 2016), and more general cloud 3D effects (Di Girolamo et al., 2010; Iwabuchi & Hayasaka, 2002; Marshak et al., 2006; Yang & Di Girolamo, 2008) on pixel-level retrievals. Although a few studies showed that how pixel-level biases from liquid water cloud retrievals impact higher-level products (Grosvenor & Wood, 2014; Horváth et al., 2014; Liang et al., 2015), very little is known about impacts on global ice clouds. The primary objective of this study is to fill the knowledge gap between biases on the pixel-level and higher-level ice cloud products.

Operational retrievals from the Moderate Resolution Imaging Spectroradiometer (MODIS, Platnick et al., 2017) are utilized in the present investigation. MODIS is an imager with which visible near-infrared (VNIR) and shortwave infrared (SWIR)/midwave infrared reflectances are used to infer daytime cloud properties (e.g., Nakajima & King, 1990; Twomey & Cocks, 1989). For practical reasons, the VNIR/SWIR method based on the PPH assumption has been widely applied to a large number of satellite-based (Buriez et al., 2005; Minnis et al., 2011; Roebeling et al., 2006; Rossow & Schiffer, 1999) and airborne imagers (Meyer et al., 2016). Meanwhile, the MODIS Level-3 products (King et al., 2013; Platnick et al., 2017) are frequently used in model evaluations (Otkin & Greenwald, 2008), improving model microphysics schemes (Barahona et al., 2014), and other climate-related studies (Zhou et al., 2013). This study focuses on how pixel-level retrieval biases from MODIS-like passive satellite imagers due to ice cloud vertical heterogeneity (ICVH) effects impact the Level-3 products. MODIS ice cloud optical thickness (COT), IWP, and calculations of broadband reflected shortwave radiation (RSR) and outgoing longwave radiation (OLR) at the top of the atmosphere (TOA) are used as vertically integrated proxies to estimate the effects quantitatively. Only the ICVH is investigated in this study for two reasons. First, cloud horizontal heterogeneity effects on scales larger than a pixel can be well represented in Level-3 products by introducing joint histograms of retrieval variables rather than only providing basic statistics such as their averages and standard deviations. Indeed, joint histograms of COT and cloud effective radius (CER), and COT and cloud-top pressure are explicitly

provided in the MODIS 8-day and monthly 1 × 1° products (Hubanks et al., 2016). Second, biases associated with cloud 3D effects are mainly dependent on incident-viewing geometries. For example, the sign of retrieval bias due to cloud-side illumination changes when the incident-viewing geometry varies from forward scattering (scattering angle toward 0°) to backward scattering (scattering angle toward 180°). It is therefore expected that the biases will average out to some extent when a large pixel sample size is used.

The present study first introduces pixel-level ICVH biases in terms of different ice cloud properties due to the PPH approximation with a theoretical experiment, which is discussed in section 2. This study then shows how the pixel-level ICVH effects propagate to Level-3 statistics by using cloud retrievals from Collection 6 (C6) Aqua-MODIS, Cloud Profiling Radar on board CloudSat (Stephens et al., 2002), and Cloud-Aerosol Lidar with Orthogonal Polarization on board Cloud-Aerosol Lidar and Infrared Pathfinder Satellite Observation (CALIPSO, Winker et al., 2013). More details about the method, data, and results are shown in section 3. Discussion and conclusions are given in sections 4 and 5.

2. Theoretical Analysis

Impacts from the cloud vertical heterogeneity on passive satellite remote sensing have been well studied during the past several decades for liquid water clouds (e.g., Chen et al., 2007; Miller et al., 2016; Platnick & Valero, 1995; Platnick, 2000; Zhang, Platnick, et al., 2010; Zhang, Wang, et al., 2010) and for ice clouds (e.g., van Diedenhoven et al., 2016). Therefore, a similar theoretical experiment is introduced here to understand how MODIS-like passive ice cloud retrievals are biased with different degrees of the ICVH.

The MODIS C6 (Platnick et al., 2017) ice COT (scaled to the 0.64-μm channel) and CER are simultaneously retrieved using reflectance from a weak absorbing VNIR channel, which is mostly determined by COT, and reflectance from an absorbing SWIR channel (e.g., 2.1 μm for MODIS and 2.25 μm for Visible Infrared Imaging Radiometer Suite, Wang et al., 2018), which generally is a function of both COT and CER. For ice clouds over open ocean (without sea ice), the MODIS C6 product provides three separate COT and CER retrievals using the channel pairs 0.86 and 2.1 μm, 0.86 and 1.6 μm, and 0.86 and 3.7 μm. The MODIS 3.7-μm reflectances are used after removing thermal emission. A cloud macrophysical variable IWP is defined as the vertical integral of ice mass per unit area,

$$\mathrm{IWP} = \rho_{\mathrm{ice}} \int_{\mathrm{Cloud-base}}^{\mathrm{Cloud-top}} \int_{r_{\min}}^{r_{\max}} \mathrm{V}(r,z)\mathrm{N}(r,z)\mathrm{d}r\mathrm{d}z, \tag{1}$$

where ρ_{ice} is the density of ice crystals, V(r, z) and N(r, z) are the total volume of ice mass (e.g., no bubble and/or hollow cavity) and number density of ice particles with radius r at height z, respectively. IWP can be expressed as a function of ice COT and CER under the PPH assumption,

$$\mathrm{IWP} = \gamma \times \rho_{\mathrm{ice}} \times \mathrm{COT} \times \mathrm{CER}. \tag{2}$$

The parameter γ is determined by the vertical profiles of ice particle size distribution (Miller et al., 2016; Seethala & Horváth, 2010; Wood & Hartmann, 2006). For vertically homogeneous ice cloud, in which CER is a constant, γ is close to 0.67. MODIS also explicitly provides three IWPs using successful (e.g., a valid COT/CER pair can be found in the solution space) COT and CER retrievals from the three channel pair combinations by following equation (2).

In this section, we conduct MODIS-like retrievals for vertically heterogeneous ice clouds using synthetic reflectances at 0.86, 1.6, 2.1, and 3.7 μm that are calculated with the Discrete Ordinates Radiative Transfer (DISORT) code (Stamnes et al., 1988). Each simulated ice cloud is divided into 11 sublayers to capture CER vertical variations and coupled with 11 idealized CER profiles. Examples of model simulated ice cloud Nakajima-King lookup tables, and SW albedo and OLR spectra at the TOA for different CER profiles are shown in the supporting information (Figures S1 and S2). Consistent with MODIS C6 ice radiative model assumptions (Platnick et al., 2017; Yang et al., 2013), ice particles are assumed to be column aggregates with severely roughened surfaces and satisfy a gamma distribution with an effective variance of 0.1. An optimal estimation-based retrieval method (Rodgers, 2000) is used to infer COT, CER, and the derived IWP using the PPH assumption. Only column integrated scalars COT and IWP are selected in comparison between the MODIS-like retrievals and the *truth* because there is no single definition of a scalar CER for a vertically

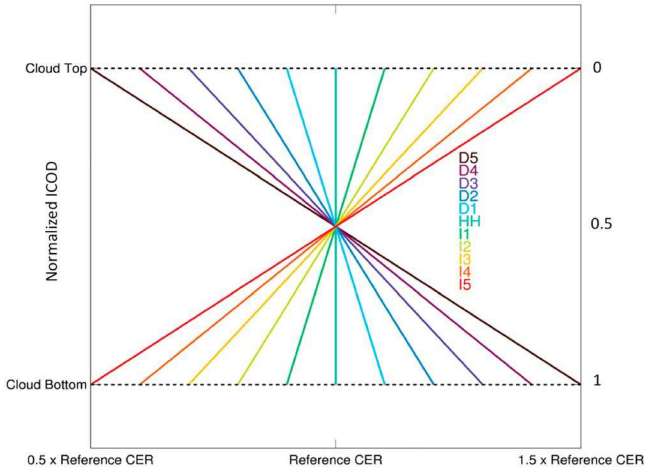

Figure 1. Illustration of the 11 idealized CER profiles. CER linearly varies with in-cloud optical depth (ICOD) for each profile. A CER profile is labeled with *Ix* (warm color), *Dx* (cold color), or *HH* (green) if CER increases, decreases, or remains constant with height. CER = cloud effective radius.

heterogeneous cloud. The 11 idealized CER profiles, as shown in Figure 1, specify profiles that vary linearly with in-cloud optical depth (ICOD). A CER profile is labeled with *I1-I5*, *D1-D5*, or *HH* if CER increases, decreases, or remains constant with height (or opposite for ICOD), respectively. A larger (smaller) number associated with a profile label indicates a larger (smaller) CER variation with ICOD. Although profiles D1-D5 are more realistic according to CALIPSO/CloudSat observations (see section 3), investigations of profiles I1-I5 are included in the theoretical analysis for a complete understanding of ICVH effect. A reference (or column averaged) CER is defined for vertically heterogeneous ice cloud as

$$\overline{\mathrm{CER}} = \frac{\sum_{i=1}^{11} \mathrm{CER}_i \mathrm{COT}_i}{\sum_{i=1}^{11} \mathrm{COT}_i} \propto \frac{\mathrm{IWP}}{\mathrm{COT}}, \tag{3}$$

where COT_i and CER_i are COT and effective radius of the ith sublayer, respectively. With this definition, it is important to emphasize that IWPs from the 11 CER profiles are identical for the same COT and reference CER.

Pixel-level retrieval uncertainties are estimated by assigning a 5% radiometric uncertainty, a 3% surface albedo uncertainty, and a 15% water vapor profile uncertainty. The ice cloud is located between 8 and 9 km in a midlatitude summer atmosphere, and Rayleigh scattering is only considered for the 0.86-μm channel. More details about the retrieval configuration are listed in Table 1. Figures 2 and 3 show COT and IWP retrievals using the three MODIS channel combinations, respectively. The MODIS-like retrievals are reliable since the normalized cost functions for all profiles are small. The solution is expected to be unique because, according to our experience with the MODIS C6 ice crystal habit, the retrieval solution space is unlikely to overlap (see Figure S1). As expected, the ICVH (horizontal axes) has little impact on the COT retrieval regardless of channel selection, with COT retrieval biases near zero across the range of vertical structures and optical thicknesses. The COT retrieval uncertainties caused by the aforementioned radiometric and model uncertainties are confined in a ±20% range and also show little variation (less than 1%) among the 11 vertical structures. Unlike COT, the IWP retrieval is more readily influenced by the ICVH. Absorption of ice crystals in SWIR channels means retrieved CERs are weighted toward cloud top (Platnick, 2000), leading to negative (positive) biases when cloud top CERs are smaller (larger). The ICVH impact becomes more significant when the cloud is optically thick (e.g., COT greater than 20) and a severely heterogeneous profile (e.g., D5 or I5) is considered, leading to an approximately ±40% IWP bias. Comparison among the three channel combinations shows that the 3.7-μm channel retrieval has the largest IWP bias, due to ice crystals being more absorptive in this channel (Yang et al., 2013).

Table 1
Configuration of the OE-Based COT and CER Retrieval Algorithm

Retrieval inputs	Variables	Uncertainty
Surface albedo	5%	3%
Temperature profile	Midlatitude summer [a]	1 K
Water vapor concentration profile	Midlatitude summer	15%
Reflectances at 0.86, 1.6, 2.1, and 3.7 μm	Simulated with DISORT	5%
Viewing zenith angle	30°	-
Solar zenith angles	0–80° with a 10° interval	-
Relative azimuthal angle	60°	-
Ice cloud location	8–9 km	-

Note. DISORT = Discrete Ordinates Radiative Transfer; OE = optimal estimation; COT = cloud optical thickness; CER = cloud effective radius.
[a]Standard midlatitude summer profile (McClatchey et al., 1972).

Figure 4 shows IWP retrievals for a range of solar zenith angles (SZAs). This experiment demonstrates that, in addition to the degree of the ICVH that gradually impacts IWP retrievals from the homogeneous cloud (HH) to severely heterogeneous (D5) cloud (panels from left to right), an oblique incident angle also enhances the ICVH impact by increasing the possibility of incident photons absorbed by the upper part of a cloud. The overall IWP biases due to the ICVH vary from 5% for slightly heterogeneous clouds (e.g., D1) to 40% for severely heterogeneous clouds (e.g., D5). Additional 10% biases are superimposed on IWP retrievals by the secondary factor SZA.

3. Impacts of the ICVH on Global Ice Cloud Records From MODIS Retrievals

With impacts of the ICVH on pixel-level retrievals in mind, it is still unclear whether such impacts are significant for specific uses. For example, how can the effects associated with the ICVH in satellite Level-3 cloud

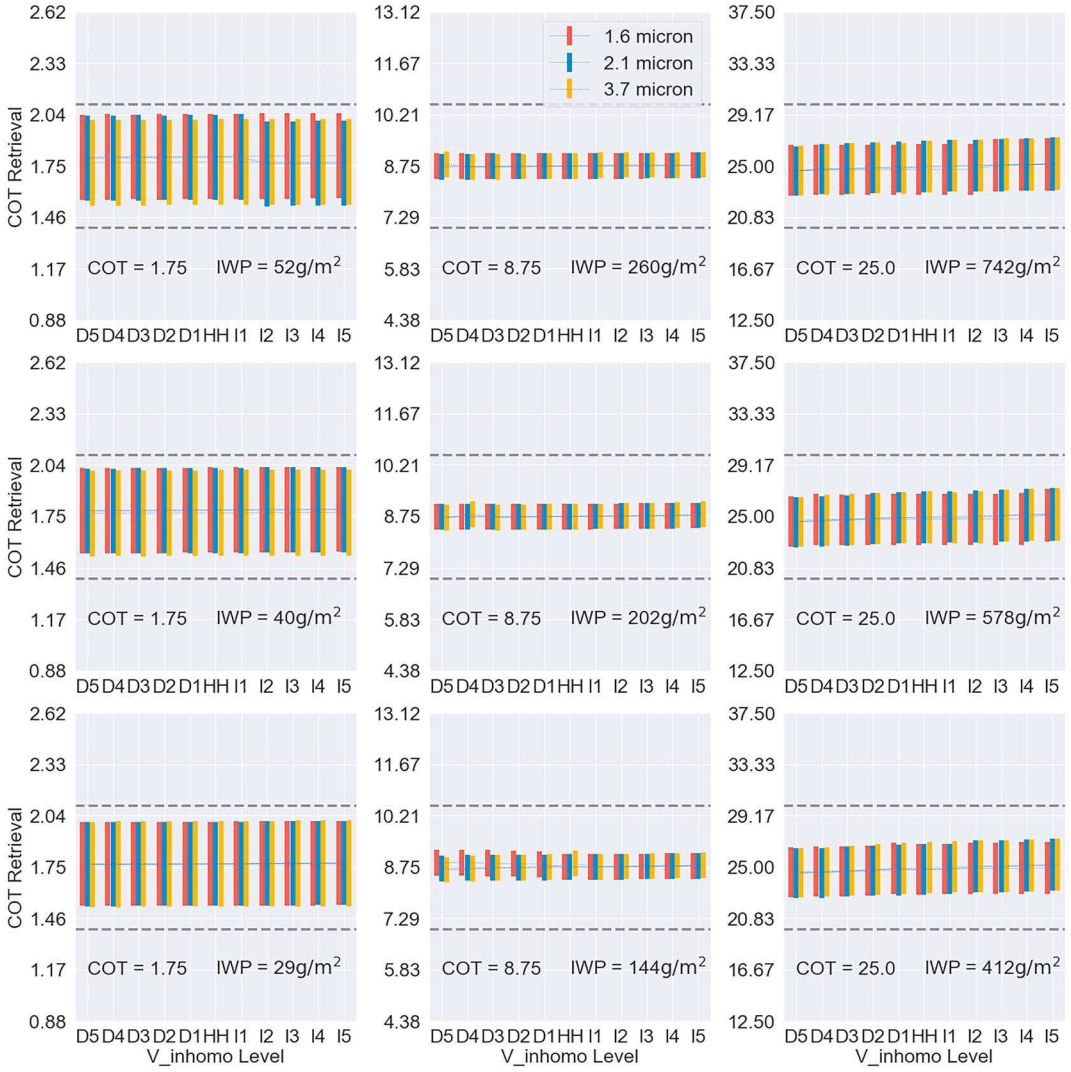

Figure 2. Retrieved COTs (solid curves) and uncertainties (error bars) for different CER profiles. Reference COT and IWP are given in each panel. Retrievals based on different channel combinations are shown in blue (0.86 and 2.1 μm), red (0.86 and 1.6 μm), and yellow (0.86 and 3.7 μm), respectively. The two dash lines in each panel indicate ±20% COT errors. Solar zenith angle is 30°. Other configurations are given in Table 1. COT = cloud optical thickness; IWP = ice water path; CER = cloud effective radius.

aggregation products be estimated? How and to what degree do such effects impact derived cloud radiative properties? To answer these questions, we link pixel-level biases with MODIS monthly mean cloud products (e.g., Level-3 MYD08_M3) by using more realistic ice cloud vertical structures extracted and parameterized from 1-year joint CALIPSO/CloudSat observations (see section 3.1). The monthly mean Level-3 quantities assessed in this study include IWP and ice cloud SW and longwave (LW) radiative effects. The impact on COT is not studies since little impact is found in the theoretical experiment (see section 2).

3.1. Parameterization of Global Ice Cloud Vertical Structure

In contrast to passive satellite sensors that only observe column-integrated or column-weighted cloud properties, CALIPSO and CloudSat, as part of the A-Train satellite constellation, are equipped with active sensors that provide a curtain view of global clouds (Stephens et al., 2002; Winker et al., 2013). Using the data set of Khatri et al. (2018), 1 year of the CALIPSO/CloudSat 2B-GEOPROF-LIDAR (Mace & Zhang, 2014) and 2C-ICE (Deng et al., 2010, 2015) products from 2007 provides statistics of global ice cloud vertical structure including altitude, 532-nm extinction coefficient profiles, ice water content (IWC), and CER profiles. Details

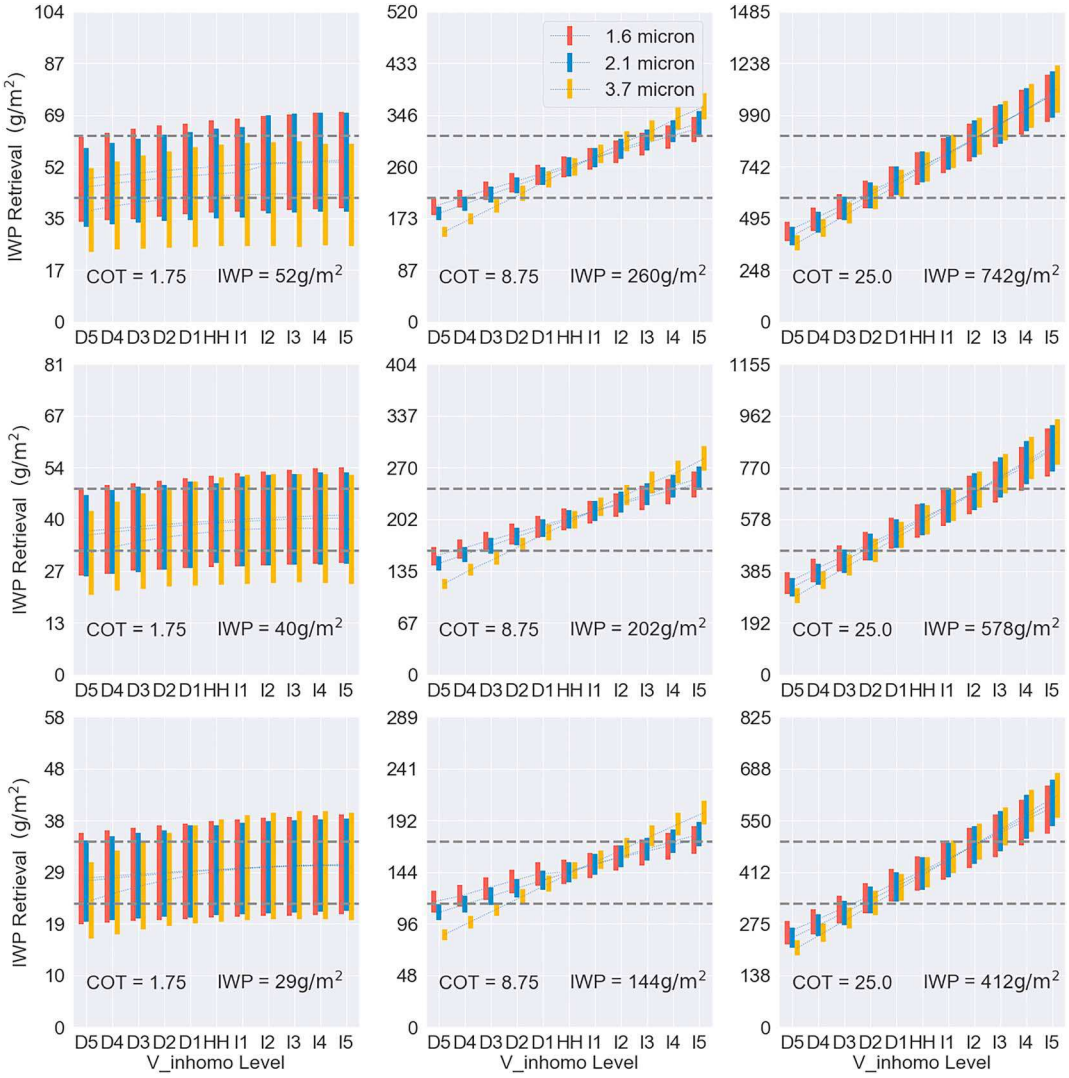

Figure 3. Same as Figure 2 except IWP retrieval biases and uncertainties are shown. COT = cloud optical thickness; IWP = ice water path.

about the development of the ice cloud statistics are given in Khatri et al. (2018). Figure 5 shows IWC and CER profiles as function of normalized in-cloud geophysical depth. The individual profiles are normalized to make the largest values in each IWC and CER value equal to 1. The joint CALIPSO/CloudSat observations show that ice clouds with different IWPs have different vertical structures. For clouds with IWP less than 10 g/m^2, CER is quasi-constant in the vertical direction. However, for clouds with higher IWPs, larger particles are always found near cloud base. This feature is consistent with previous studies (Feofilov et al., 2015; Ham et al., 2013). Figure 6a is the same as Figure 5b, but the *y* axis is converted to normalized ICOD. It is clear that the CER-ICOD profiles are nonlinear when CloudSat IWPs are larger than 300 g/m^2 (yellow, orange, and red curves in Figure 6a). Actually, Ham et al. (2013) showed that the nonlinear structures of CloudSat IWC/CER profiles are highly correlated with deep convective clouds. The relative locations of maximum IWC/CER for deep convective clouds could be higher than other ice cloud types due to the strong upward motion. However, for deep convective clouds (or larger IWP cases), the CER/IWC profiles from CloudSat near cloud bases always have larger uncertainties (Deng et al., 2010; Ham et al., 2013). For this reason, we still use a linear regression to represent the CER-ICOD profiles for different IWPs for simplification in this study. Once all CER slopes are calculated for different IWPs, a two-degree polynomial regression is used to fit the IWP-CER slope curve, as shown in Figure 6b:

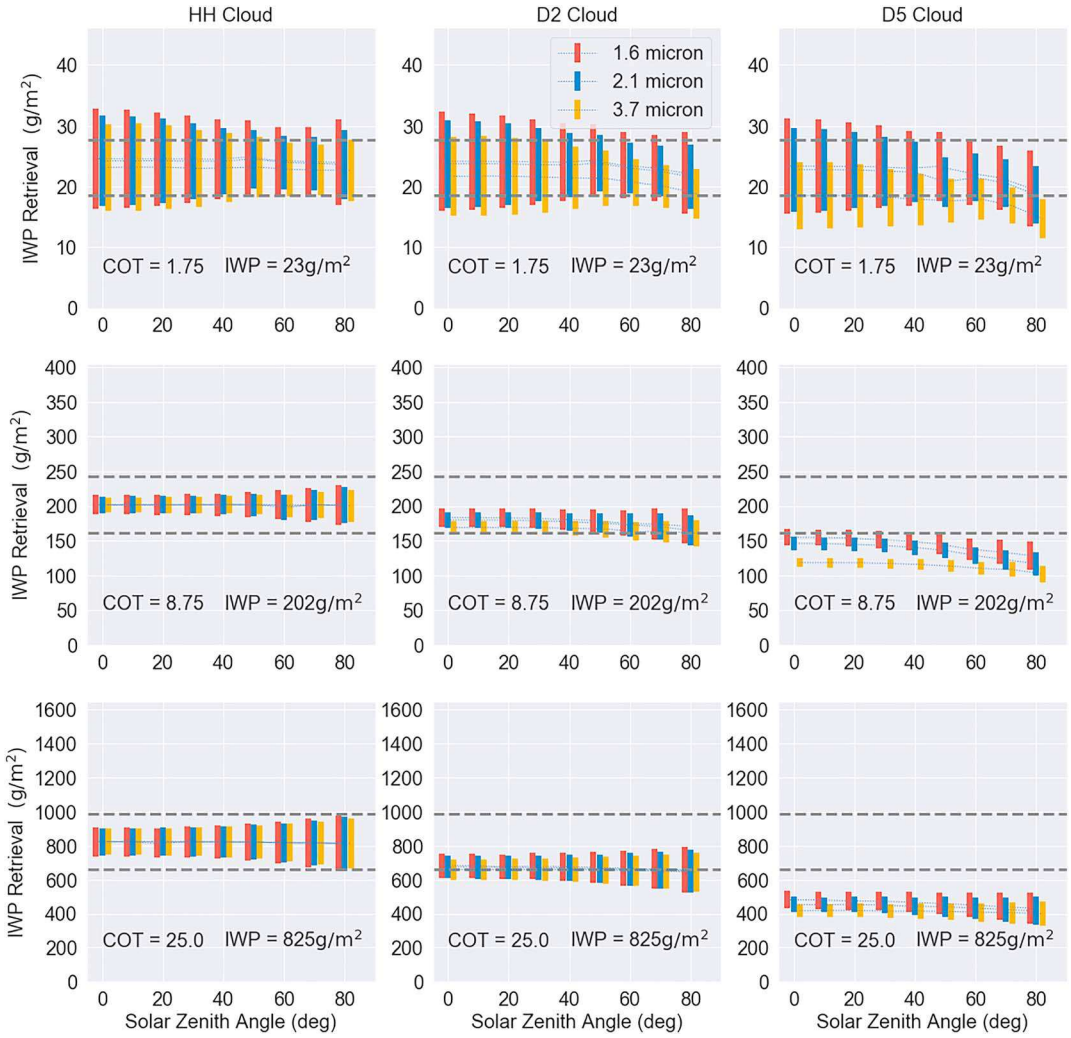

Figure 4. Retrieved IWPs (solid curves) and uncertainties (error bars) for different CER profiles and SZAs. Degree of the ICVH effect increases from the left column (homogeneous clouds) to right columns (D2 and D5). Other configurations are the same with Figures 2 and 3. IWPs = ice water paths; CER = cloud effective radius; SZAs = solar zenith angles; ICVH = ice cloud vertical heterogeneity.

$$\text{slope} = ax^2 + bx + c, \tag{4}$$

where x represents ln(IWP), and the three fitting coefficients a, b, and c are 0.06, −0.92, and 4.94, respectively.

3.2. Estimating the ICVH Effects on MODIS Level-3 IWP

The Aqua-MODIS C6 Level-3 monthly product (MYD08_M3) provides joint histograms in 12 × 11 COT-CER bins on 1 × 1° grids (Platnick et al., 2017), in addition to scalar statistics. For consistency, in this study we first calculate MODIS-like observations at 0.86, 1.6, 2.1, and 3.7 μm for vertically heterogeneous ice clouds at the 12 reference COTs and 11 reference CERs (defined in equation (3)) using DISORT. The relationship between IWP and CER profiles is established on the basis of the aforementioned parameterization scheme (equation (4)). Three spectral MODIS-like PPH retrievals are obtained from the simulated heterogeneous observations. Figure 7 shows examples of comparisons among the three simulated retrievals (IWP_{MODIS}) and the references (IWP_{ref}, i.e., unbiased IWP) as a function of IWP. As expected, most IWP_{MODIS} values are underestimated as a result of the prevailing CER profile (e.g., small particles near cloud top) suggested by CALIPSO/CloudSat. The 3.7-μm IWP_{MODIS} values are systematically lower than the other two retrievals, especially when IWP_{ref} values are between 50 and 500 g/m^2, due to the relatively stronger ice crystal

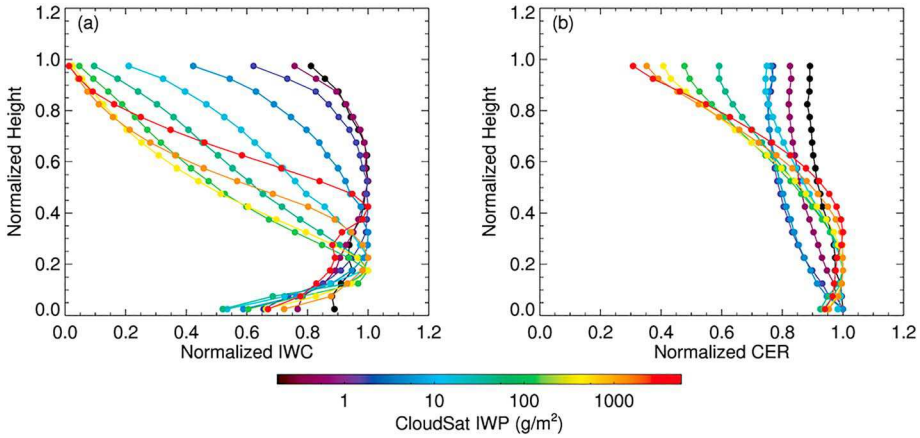

Figure 5. IWC (a) and CER (b) profiles as a function of normalized in-cloud geophysical thickness (0 at cloud-bottom and 1 at cloud-top), derived from 1-year joint CALIPSO/CloudSat observations (2B-GEOPROF-LIDAR and 2C-ICE) in 2007. IWC and CER profiles are normalized to make the highest IWC/CER value in each profile equal to 1. More details about the profile data sets are discussed in Khatri et al. (2018). CER = cloud effective radius; IWC = ice water content; CALIPSO = Cloud-Aerosol Lidar and Infrared Pathfinder Satellite Observation.

absorption. The largest negative IWP biases for all three IWP_{MODIS} retrievals are found at large SZAs. Another 2° polynomial regression is used to estimate the IWP_{ref} from the IWP_{MODIS}:

$$\ln(\mathrm{IWP_{ref}}) = c_1(\mu_0)[\ln(\mathrm{IWP_{MODIS}})]^2 + c_2(\mu_0)[\ln(\mathrm{IWP_{MODIS}})] + c_3(\mu_0), \quad (5)$$

where μ_0 is the cosine of the SZA; c_1, c_2, and c_3 are three fitting coefficients that are calculated at nine different SZAs from 0 to 80° with a 10° interval. The fitting is conducted separately for each channel combination, and the fitting coefficients are provided in the supporting information (Table S1). It is expected that the monthly SZA has strong meridional and seasonal variations (see Figure S2 in the supporting information) that should be considered in global estimations of MODIS IWP biases due to the ICVH. It is important to emphasize that although viewing zenith angle (VZA) also influences pixel-level IWP retrievals, the monthly mean VZA (not shown) for a scanning imager cannot have noticeable spatial and/or seasonal variations. Therefore, a typical VZA of 30° is selected to conduct the theoretical global analyses.

In this study, we conduct IWP comparisons for global ice clouds using monthly mean cloud properties derived from successful Aqua-MODIS C6 pixel-level retrievals (MYD06_L2). To reduce large surface

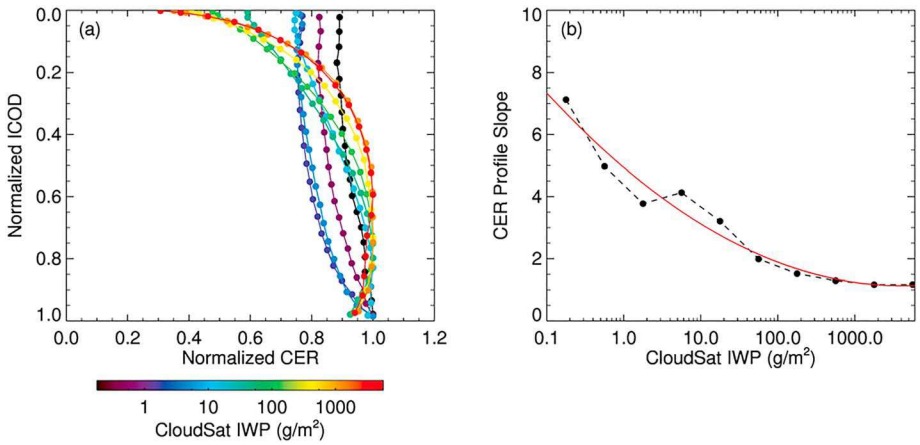

Figure 6. (a) CER profiles as a function of normalized ICOD for 10 different IWPs. CER profiles are normalized to make the highest CER value in each profile equal to 1. (b) CER-ICOD slopes derived from 10 IWPs (black dots) and a 2° polynomial regression (red curve) to fit the slope-IWP relation. CER = cloud effective radius; IWPs = ice water paths; ICOD = in-cloud optical depth.

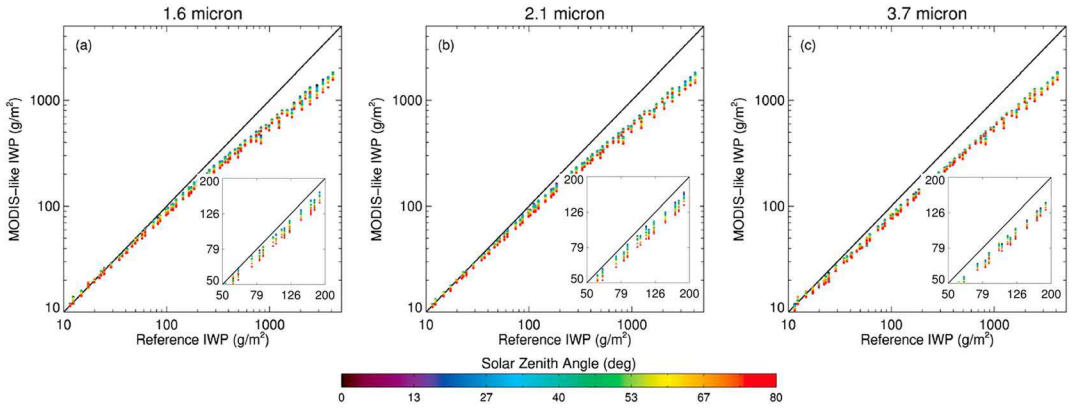

Figure 7. Comparisons between the MODIS-like retrieved IWPs and the references. Retrievals are based on simulated observations of heterogeneous ice clouds and the PPH assumption. Comparisons are conducted for different SZAs and the three channel combinations (a) 0.86 and 1.6 μm, (b) 0.86 and 2.1 μm, and (c) 0.86 and 3.7 μm. MODIS = Moderate Resolution Imaging Spectroradiometer; IWPs = ice water paths; PPH = Plane-Parallel Homogeneous; SZAs = solar zenith angles.

reflection uncertainties from land and sea ice, the global analysis is limited to oceanic grids between 60°S and 60°N. Partly cloudy (PCL) pixels are excluded from this study to mitigate 3-D effects. Global monthly mean IWPs in January and July 2007 from the C6 MODIS 2.1-μm product ($\overline{\text{IWP}}_{\text{MODIS}}$) and from the estimation ($\overline{\text{IWP}}_{\text{ref}}$) using equation (6) are shown in Figure 8. Their differences in the 2 months are shown in Figure 9. If the ICVH is the only biasing factor that influences the MODIS pixel-level products, we show that MODIS underestimates IWP by more than 30% globally except over some regions dominated by the descending branch of the Hadley cell where ice clouds have very low fractions (5% or less) and IWPs less than 100 g/m^2. Large IWP differences are strongly correlated with deep convection and high SZA regions, consistent with the theoretical analysis. Figure 10 shows the zonally averaged IWPs from the three MODIS retrievals and the corresponding references that account for the ICVH. The reference IWPs are systematically higher than their MODIS counterpart by 30% when MODIS IWPs are less than 200 g/m^2 or more than 50% when MODIS IWPs are greater than 300 g/m^2.

3.3. Radiative Impacts

Influences of the ICVH on assessing the radiation budget are quantitatively estimated in terms of ice cloudy-sky OLR (10–3,250 cm^{-1}) and RSR (0.2–5 μm). Global OLR and RSR are calculated for the MODIS retrievals and the estimated reference retrievals that account for the ICVH influences. The instM_3d_asm_Np data set (3D, monthly mean instantaneous, pressure-level, assimilated meteorological fields, version 5.12.4) from the Modern-Era Retrospective Analysis for Research and Applications, Version 2 (Gelaro et al., 2017) is utilized to provide monthly means of atmospheric profiles for the 2 months considered (January and July 2007). Although the MODIS C6 MYD08_M3 product provides COT-CER and COT-cloud top temperature joint histograms for ice clouds, in this study, monthly mean daytime cloud-top heights (CTHs), SZAs, and joint COT-CER and COT-CTH histograms are calculated directly from MODIS non-PCL retrievals (MYD06_L2) at a horizontal resolution of 1 × 1°. Gas absorption, Rayleigh, and ice crystal scattering are calculated by coupling a line-by-line radiative transfer model (Clough et al., 2005) and DISORT (Stamnes et al., 1988). A global data set of surface spectral emissivity (Chen et al., 2014; Huang et al., 2016) is used in the OLR calculation. Note that in the flux calculations, we also use 11 sublayers in DISORT to capture the vertical variation of ice CER. To emphasize the ICVH impact, in this study, ice cloudy-sky OLR and RSR are used rather than all-sky radiations. The averaged ice cloudy-sky $\overline{\text{OLR}}$ and $\overline{\text{RSR}}$ at 1 × 1° grid box index (m, n) are defined as

$$\overline{\text{OLR}}(m,n) = \frac{\sum_{i=1}^{12}\sum_{j=1}^{11}\text{OLR}\left(\overline{\text{CTH}}, \text{COT}_i, \text{CER}_j\right)\times f(i,j)}{\sum_{i=1}^{12}\sum_{j=1}^{11} f(i,j)}, \tag{6}$$

$$\overline{\text{RSR}}(m,n) = \int \frac{\sum_{i=1}^{12}\sum_{j=1}^{11}\text{RSR}\left(\overline{\text{CTH}}, \text{COT}_i, \text{CER}_j, \theta_0(t,\varphi)\right)\times f(i,j)}{\sum_{i=1}^{12}\sum_{j=1}^{11} f(\text{i},j)}\text{d}t, \tag{7}$$

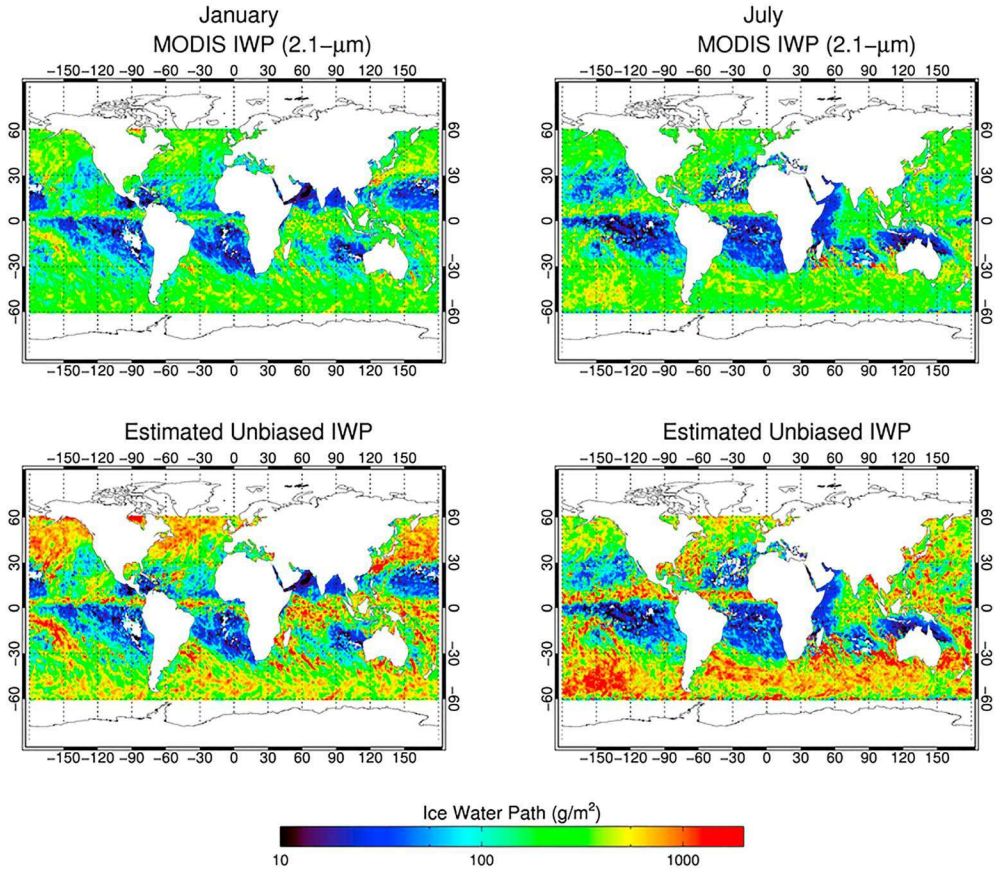

Figure 8. The monthly mean MODIS 2.1 μm (first row) and the estimated reference IWPs (second row) in January (left column) and July (right column) 2007. MODIS = Moderate Resolution Imaging Spectroradiometer; IWPs = ice water paths.

where $f_{i,j}$ is the all-sky fraction of ice cloud in the ith COT bin and jth CER bin, $\overline{\mathrm{CTH}}$ is the monthly mean CTH, and θ_0 is the SZA, which is a function of local time t and latitude φ. Note that, because we are only interested in the relative impact of the ICVH on OLR and RSR, equations (6) and (7) use the implicit assumption that the observed ice cloud properties and cloud fractions do not have a diurnal variation. Figure 11 (top row) shows ice cloudy-sky OLRs derived directly from the MODIS 2.1-μm retrievals in January (left) and July (right) 2007. The ice cloudy-sky OLR differences, defined as the $\overline{\mathrm{OLR}}_{\mathrm{MODIS}}-\overline{\mathrm{OLR}}_{\mathrm{ref}}$, for these 2 months are shown in the bottom row. Only small OLR differences, within ±1 W/m^2 (or less than ±1% relative), are found despite the large IWP differences shown in Figures 9 and 10. Most high ice cloud fraction regions are dominated by positive OLR differences except for regions with low Sun angles (above 30°N in January, below 30°S in July).

Global ice cloudy-sky RSRs from the MODIS 2.1-μm retrievals, and their estimated differences from RSRs calculated from the reference retrievals, are shown in Figure 12. Similar to the OLR comparisons, relatively small impacts (±1 W/m^2) from the ICVH are found on global RSR calculations. However, the spatial patterns of the RSR differences are more complicated than the OLR differences. Generally, a positive RSR difference ($\overline{\mathrm{RSR}}_{\mathrm{MODIS}}-\overline{\mathrm{RSR}}_{\mathrm{ref}}$) is linked to a high IWP value (e.g., $\mathrm{IWP}_{\mathrm{ref}} > 500\mathrm{g/m}^2$) and a negligible RSR difference can be found at a low IWP value (e.g., $\mathrm{IWP}_{\mathrm{ref}} < 100\mathrm{g/m}^2$). A notable negative RSR difference (−0.5 to − 1W/m^2) frequently occurs when the cloud is moderately thick (e.g., 100 g/m^2 < $\mathrm{IWP}_{\mathrm{ref}}$ < 500g/m^2). The total flux (OLR + RSR) differences, averaged for ice clouds with different IWPs, are shown in Figure 13. Interestingly, for IWP less than 500 g/m^2, the global negative RSR differences are offset by positive OLR differences, resulting in small total flux differences; for IWP greater than 500 g/m^2, the RSR difference is positive and dominates the OLR difference. Total flux differences are positive (up to 0.29 ± 0.24 W/m^2) for almost all oceanic ice clouds, with the exception of those having IWP less than 100 g/m^2.

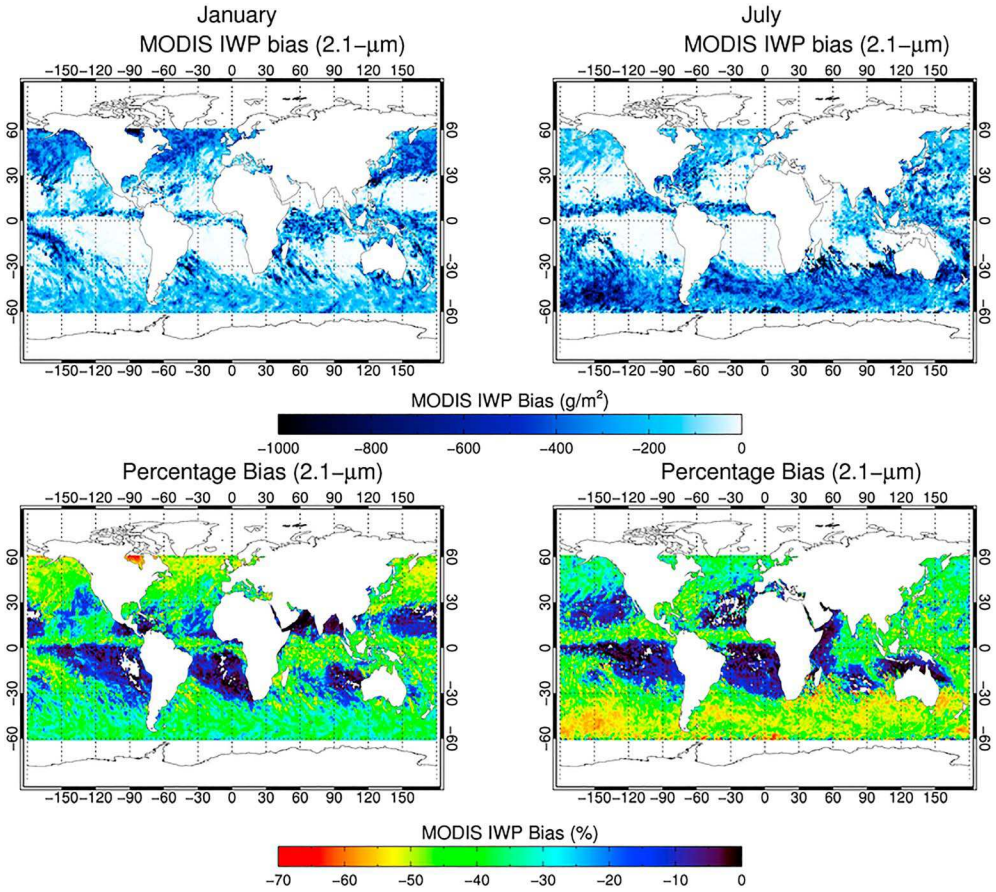

Figure 9. The absolute (first row) and relative (second row) differences of monthly mean IWPs between the MODIS 2.1 μm and estimated reference IWPs in January (left column) and July (right column) 2007. MODIS = Moderate Resolution Imaging Spectroradiometer; IWPs = ice water paths.

4. Discussion

4.1. IWP, RSR, and OLR Differences

Global analysis of the ICVH impacts shows that MODIS-like ice cloud products, based on the PPH retrievals, have lower IWPs in comparison to reference IWPs using parameterized CER vertical variations. As discussed with regard to the theoretical calculations, IWPs from MODIS-like retrievals (IWP_{MODIS}) are always lower

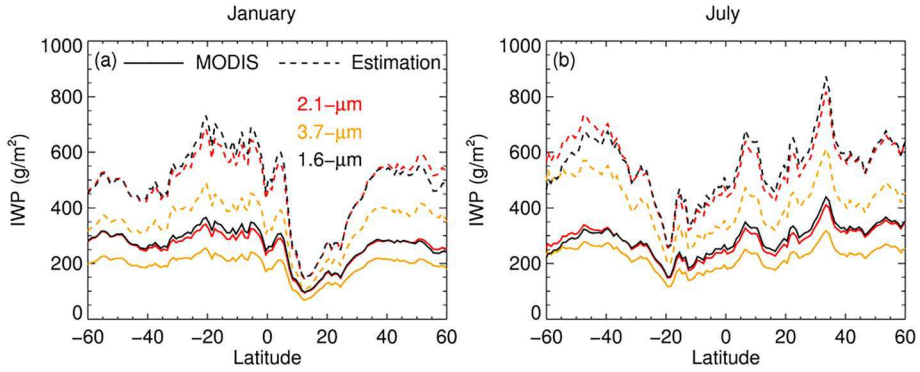

Figure 10. Zonal mean IWPs from the three MODIS retrievals (solid curves) and corresponding estimated references (dashed curves) in January (a) and July (b) 2007. Retrievals and corresponding estimated references are shown in different colors: Red (0.86 and 2.1 μm), black (0.86 and 1.6 μm), and yellow (0.86 and 3.7 μm). MODIS = Moderate Resolution Imaging Spectroradiometer; IWPs = ice water paths.

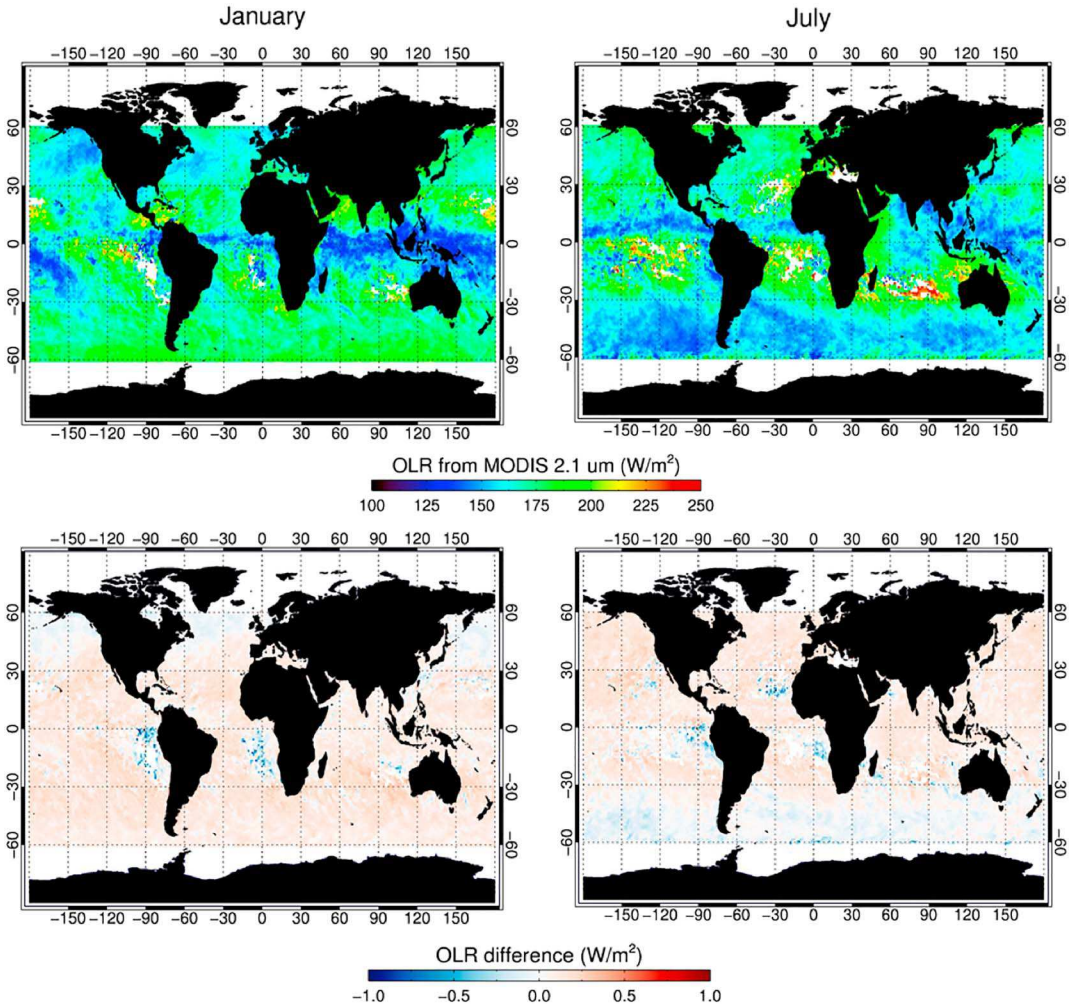

Figure 11. Ice cloudy-sky OLRs calculated using the MODIS (2.1 μm) cloud retrievals (first row) and OLRs differences between the MODIS (2.1 μm) and the reference OLRs (second row) in January (left column) and July (right column) 2007. MODIS = Moderate Resolution Imaging Spectroradiometer; OLRs = outgoing longwave radiations.

than the reference IWPs (IWP_{ref}), largely because the CER retrieved from passive sensors is more or less weighted toward the upper parts of ice clouds. The expected IWP bias (i.e., $IWP_{MODIS} - IWP_{ref}$) is approximately proportional to the magnitude of IWP_{ref}. This results from larger IWPs having a higher likelihood of large CER vertical gradients as indicated by joint CALIPSO/CloudSat observations. In addition to CER vertical structure, SZA plays a secondary role in biasing MODIS-like IWP retrievals. The combined effects result in large negative IWP differences, especially in deep convection, and middle to high-latitude regions in the winter hemisphere. The ICVH effect, albeit incomplete, may partly explain retrieval diversity between passive and active retrievals and other estimates of IWP (see Figure 1 in Duncan & Eriksson, 2018).

The sign of the RSR difference changes from negative (optically thin clouds) to positive (optically thick clouds) as shown in Figures 13b and 13d. This feature is illustrated more clearly in Figure 14, which shows instantaneous SW flux differences at the 12 × 11 COT-CER bins assuming a SZA of 60°. Small negative RSR differences are found for ice clouds with MODIS COT less than 15, while large positive RSR differences occur when MODIS COT is larger than 50. The sign and magnitude of the RSR differences are determined by two competing factors: the COT spectrum and IWP (or column-averaged CER). For optically thin ice clouds, the IWP differences between the MODIS and reference values are small, and therefore, COT differences in 0.4- to 0.6-μm spectral range contribute most to the RSR differences. Figure 15 shows that, although COTs at 0.64 μm in the two RSR calculations are the same since the ICVH has little impact on MODIS COT retrievals (COT ratios, defined as the reference COT to MODIS-like COT, are 1 at 0.64 μm), the reference COTs are

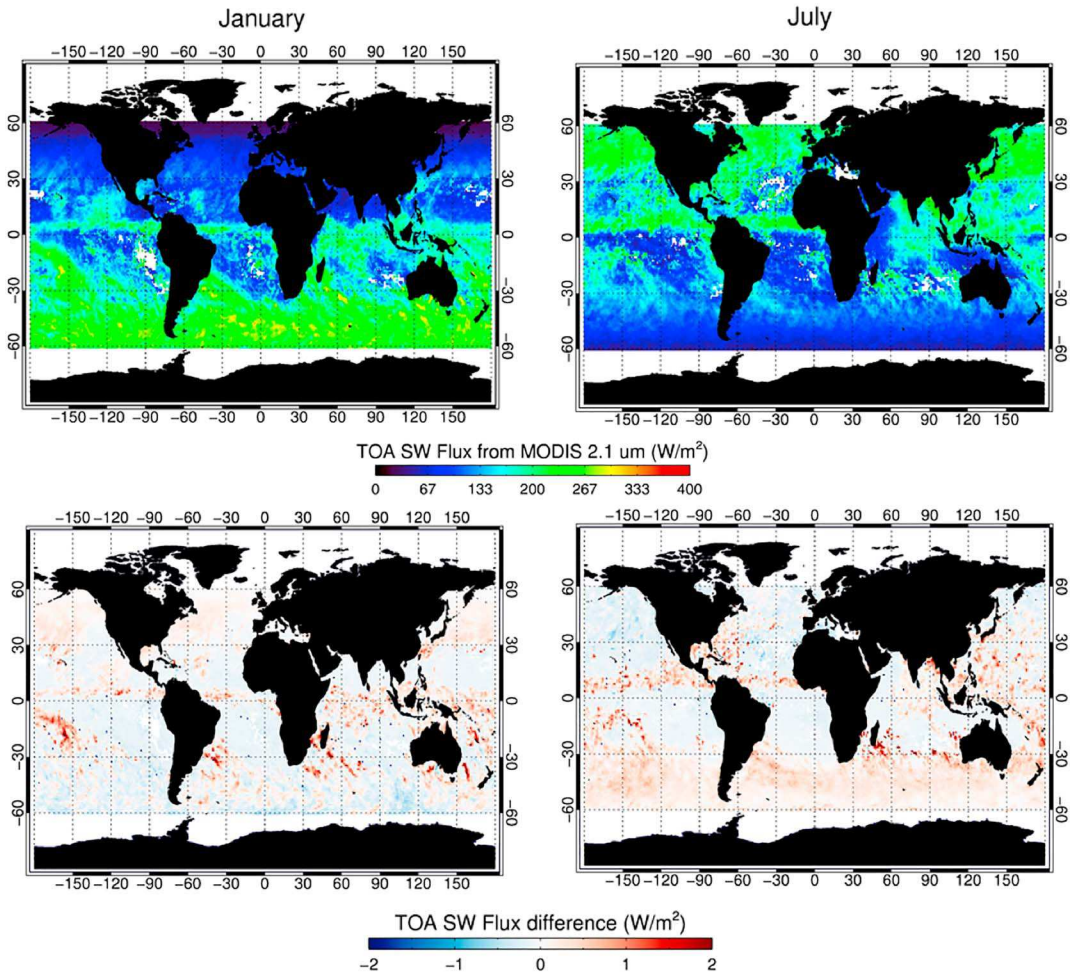

Figure 12. Same as Figure 11 except RSRs and corresponding RSR differences are shown. RSRs = reflected shortwave radiations; SW = shortwave; TOA = top of the atmosphere.

larger than the MODIS COTs from 0.2 to 0.6 μm due to the change of CER profiles. The resulting larger reference COTs yield a larger SW albedo between 0.2 and 0.6 μm. However, for optically thick clouds with COT larger than 30, the RSR spectrum (0.2 to 0.6 μm) is no longer sensitive to COT due to the saturation of VNIR reflection. Under this condition, the different IWPs contribute most to the RSR differences in the NIR through the SWIR spectral region. Larger reference IWPs make clouds dimmer (lower RSR) in the NIR through the SWIR region due to cloud absorption. The OLR differences are largely caused by COT

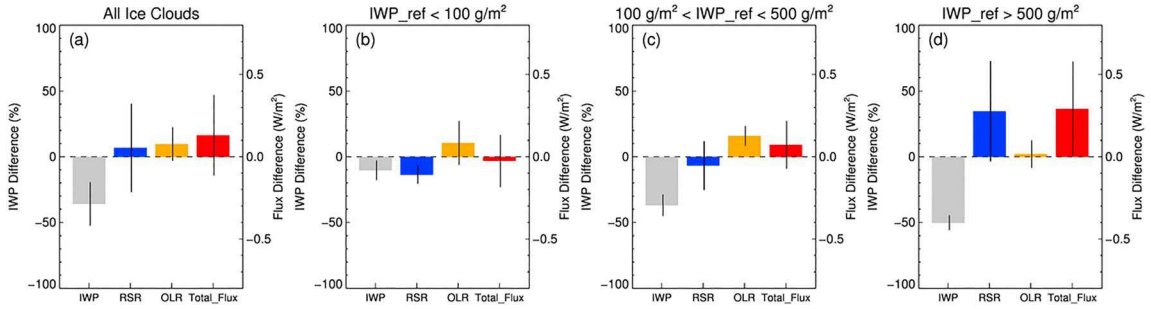

Figure 13. Estimated impacts of the ICVH on IWP retrievals (gray), and further derived ice cloudy-sky RSRs (blue), OLRs (yellow), and total fluxes at the top of the atmosphere (RSR + OLR, red) for (a) all ice clouds, (b) ice cloud with $IWP_{ref} < 100$ g/m^2, (c) $100 < IWP_{ref} < 500$ g/m^2, and (d) $IWP_{ref} > 500$ g/m^2. RSR = reflected shortwave radiation; ICVH = ice cloud vertical heterogeneity; OLR = outgoing longwave radiation; IWP = ice water path.

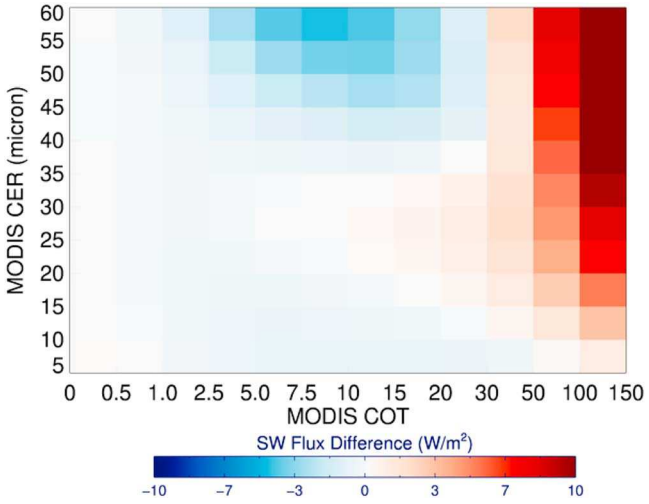

Figure 14. Instantaneous SW flux difference between the RSR from the MODIS (2.1 μm) and corresponding reference at the 12 × 11 COT-CER bins with SZA at 60°. MODIS = Moderate Resolution Imaging Spectroradiometer; SW = shortwave; SZA = solar zenith angle; CER = cloud effective radius; COT = cloud optical thickness.

differences in the IR window region (e.g., 10–12 μm). Figure 15b shows the COT ratios are greater than 1 in the IR window region, with the result being that the MODIS-retrieved clouds seem to be warmer than the reference clouds.

4.2. Limitations of This Study

Based on 1-year CloudSat/CALIPSO observation, this study estimates the ICVH effects on MODIS monthly mean ice cloud products in terms of IWP and ice cloudy-sky RSR and OLR. One limitation however is that only vertical variation of CER is considered. Indeed, a wide variety of nonspherical ice particle shapes are observed in cloud chambers (Bailey & Hallett, 2002, 2004) and field studies (Baker & Lawson, 2006; Schmitt & Heymsfield, 2010). However, it is still extremely difficult to infer ice crystal habits and/or habit profiles remotely. Actually, ice crystals with fixed habit fractions are used in the CloudSat/CALIPSO 2C-ICE product (Deng et al., 2010). Furthermore, the 1-year CloudSat/CALIPSO observation is used as a reference throughout this study, although the two active sensors also have large uncertainties in determining cloud ice profiles near the base of optically thick clouds (Deng et al., 2010; Ham et al., 2013). Therefore, we utilize a linear regression to represent CER profile for simplification. The current method may be improved in the future by utilizing different parameterization schemes for different cloud types. Another limitation of this study is that the only considered radiative impact due to the ICVH is OLR and RSR at the TOA. Further studies are needed to understand if the ICVH has a profound impact on SW and LW radiation at the surface and/or heating rate profile.

Among the three MODIS MYD06 C6 IWP products, it is evident in Figure 10 that the 3.7-μm IWPs are systematically lower than the other two spectral retrievals by up to 50%, partly due to the ICVH effects. However, obvious discrepancies are found among the three reference IWPs (see dashed curves in Figure 10) that account for the ICVH effect, suggesting that vertical heterogeneity is not the only cause of retrieval differences. For example, quality of the daytime 3.7-μm retrievals yields the accuracy of emission removal. How the ICVH impacts thermal emission at cloud top is still unclear. Mixed-phase clouds and/or supercooled liquid layer topped clouds, which are frequently observed in the intertropical convergence zone and stratiform clouds in the Southern Hemisphere from CALIPSO/CloudSat (Zhang, Platnick, et al., 2010; Zhang, Wang, et al., 2010), impact passive retrievals using different channel combinations (Miller et al., 2014). Further studies are necessary to investigate if the 3.7- to 2.1-μm IWP difference can be used as an indicator to detect mixed-phase clouds using passive sensors.

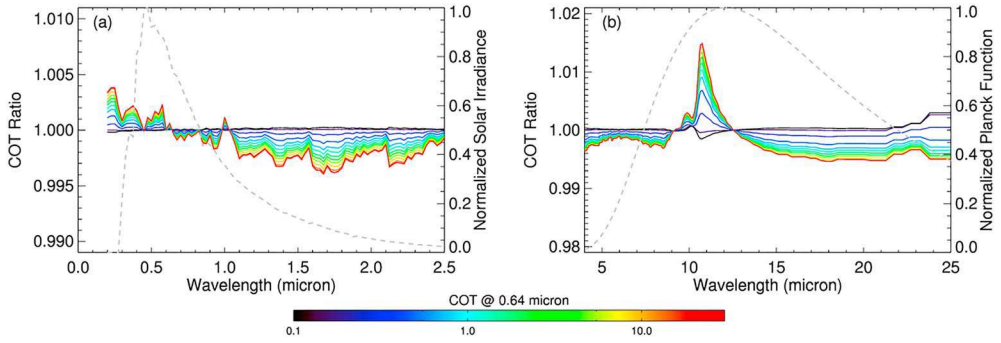

Figure 15. COT_{ref}-to-COT_{MODIS} ratio as a function of wavelength in (a) the SW, and (b) LW spectral regions. The ratio is 1 at 0.64 μm since the ICVH has little impact on MODIS-retrieved COT at this wavelength. Normalized solar irradiance and the Planck function at 240 K are shown in the SW and LW panels (gray dashed curves), respectively.
MODIS = Moderate Resolution Imaging Spectroradiometer; SW = shortwave; COT = cloud optical thickness; LW = longwave; ICVH = ice cloud vertical heterogeneity.

5. Conclusions

In order to understand how imager pixel-level PPH retrieval biases impact higher-level cloud data records, this study estimates the ICVH effects on MODIS monthly mean ice cloud products in terms of IWP, and ice cloudy-sky RSR and OLR. Cloud vertical CER profiles for ice clouds with different IWPs are parameterized using existing 1-year CloudSat/CALIPSO observations. Generally speaking, the ICVH has a substantial impact on the estimation of global IWP from passive satellite remote sensing. We show that the reference IWPs are systematically higher than their MODIS counterpart by 37% for global oceanic ice clouds (60°S and 60°N). The ICVH impact on MODIS-like IWP retrievals gradually increases with the increase of reference IWP. A large negative IWP bias (~ −50%) is found for ice clouds with large IWP_{ref} values (~ 500 g/m^2 or larger).

The present study also shows that cloud radiative properties in terms of RSR and OLR are different with different cloud vertical structures. Outgoing ice cloudy-sky fluxes in the SW (0.2–5 μm) and LW (10–3,250 cm^{-1}) spectral regions derived from the MODIS 2.1-μm retrievals and the corresponding reference with adjusted CER profiles are compared. Although obvious differences exist in terms of column-integrated cloud ice water, the line-by-line radiative transfer model + DISORT calculations show less than 1% flux differences, as long as flux calculations using the MODIS retrievals make assumptions identical to the retrievals themselves regarding, for example, the PPH approximation and the ice cloud radiative model (ice crystal habit, etc.) used in the retrieval forward radiative transfer calculations. Figure 13a shows that the MODIS-derived ice cloudy-sky RSR and OLR are slightly higher than calculations with reference ice cloud properties by 0.05 and 0.08 W/m^2 for a global average of ice clouds, suggesting that the ICVH has little impact on cloudy-sky radiation, in comparison with its large impact on IWP (37% lower globally, see gray bar in Figure 13a). The largest RSR difference (~ 2 W/m^2) is largely associated with deep convective regions where typical IWP is larger than 2,000 g/m^2 (see Figure 12). Overall, the RSR comparison shows a slight negative RSR difference (−0.11 ± 0.05 W/m^2) for ice clouds with IWP_{ref} less than 100 g/m^2 and a positive RSR difference (0.27 ± 0.30 W/m^2) for ice clouds with IWP_{ref} greater than 500 g/m^2. This impact is rather trivial in comparison with other artificial effects that bias cloud radiative properties. For example, ignoring LW scattering can introduce a 2–3 W/m^2 bias in estimating global cloud OLR (Costa & Shine, 2006; Kuo et al., 2017). Selecting different ice crystal models may introduce a larger SW flux difference (e.g., 20 W/m^2 or greater) according to previous studies (Yang et al., 2007; Yi et al., 2017; Zhang et al., 2009).

Acknowledgments
The authors are grateful for support from the NASA Radiation Sciences Program. The computations in this study were performed at the UMBC High Performance Computing Facility (HPCF). The facility is supported by the U.S. National Science Foundation through the MRI program (grants CNS-0821258 and CNS-1228778) and the SCREMS program (grant DMS 0821311), with additional substantial support from UMBC. The Collection 6 MODIS products (doi: http://dx.doi.org/10.5067/MODIS/MYD06_L2.006) are publicly available from the NASA and Atmosphere Archive and Distribution System (LAADS, http://ladsweb.nascom.nasa.gov). The CloudSat/CALIPSO 2C-ICE (version 4; doi:10.1002/2015JD023600) products are publicly available from the CloudSat Data Processing Center (http://www.cloudsat.cira.colostate.edu/data-products). The instM_3d_asm_Np products (3D, monthly mean instantaneous, pressure-level, assimilated meteorological fields, version 5.12.4) are from the Modern-Era Retrospective Analysis for Research and Applications, Version 2 (MERRA-2; doi: 10.1175/JCLI-D-16-0758.1) and are publicly available from the NASA Goddard Earth Sciences (GES) Data and Information Services Center (https://disc.gsfc.nasa.gov/).

References

Bailey, M., & Hallett, J. (2002). Nucleation effects on the habit of vapour grown ice crystals from −18 °C to −42 °C. *Quarterly Journal of the Royal Meteorological Society*, *128*, 1461–1484.

Bailey, M., & Hallett, J. (2004). Growth rates and habits of ice crystals between −20 °C to −70 °C. *Journal of the Atmospheric Sciences*, *61*(5), 514–544. https://doi.org/10.1175/1520-0469(2004)061<0514:GRAHOI>2.0.CO;2

Baker, B., & Lawson, R. P. (2006). Improvement in determination of ice water content from two-dimensional particle imagery. Part I: Image-to-mass relationships. *Journal of Applied Meteorology and Climatology*, *45*(9), 1282–1290. https://doi.org/10.1175/JAM2398.1

Barahona, D., Molod, A., Bacmeister, J., Nenes, A., Gettelman, A., Morrison, H., Phillips, V., et al. (2014). Development of two-moment cloud microphysics for liquid and ice within the NASA Goddard Earth Observing System Model (GEOS-5). *Geoscientific Model Development*, *7*(4), 1733–1766. https://doi.org/10.5194/gmd-7-1733-2014

Baumgardner, D., Abel, S. J., Axisa, D., Cotton, R., Crosier, J., Field, P., et al. (2017). Cloud ice properties: In situ measurement challenges. *Meteorological Monographs*, *58*, 9.1–9.23. https://doi.org/10.1175/AMSMONOGRAPHS-D-16-0011.1

Boucher, O., Randall, D., Artaxo, P., Bretherton, C., Feingold, G., Forster, P., et al. (2013). Clouds and aerosols. In T. F. Stocker et al. (Eds.), *Climate Change 2013: The Physical Science Basis. Contribution of Working Group I to the Fifth Assessment Report of the Intergovernmental Panel on Climate Change* (pp. 571–657). Cambridge, UK and New York: Cambridge University Press. https://doi.org/10.1017/CBO9781107415324.016

Buriez, J.-C., Parol, F., Cornet, C., & Doutriaux-Boucher, M. (2005). An improved derivation of the top-of-atmosphere albedo from POLDER/ADEOS-2: Narrowband albedos. *Journal of Geophysical Research*, *110*, D05202. https://doi.org/10.1029/2004JD005243

Chahine, M. T. (1992). The hydrological cycle and its influence on climate. *Nature*, *359*(6394), 373–380. https://doi.org/10.1038/359373a0

Chang, K.-W., L'Ecuyer, T. S., Kahn, B. H., & Natraj, V. (2017). Information content of visible and midinfrared radiances for retrieving tropical ice cloud properties. *Journal of Geophysical Research: Atmospheres*, *122*, 4944–4966. https://doi.org/10.1002/2016JD026357

Chen, R., Chang, F., Li, Z., Ferraro, R., & Weng, F. (2007). Impact of the vertical variation of cloud droplet size on the estimation of cloud liquid water path and rain detection. *Journal of the Atmospheric Sciences*, *64*(11), 3843–3853. https://doi.org/10.1175/2007JAS2126.1

Chen, X. H., Huang, X. L., & Flanner, M. G. (2014). Sensitivity of modeled far-IR radiation budgets in polar continents to treatments of snow surface and ice cloud radiative properties. *Geophysical Research Letters*, *41*, 6530–6537. https://doi.org/10.1002/2014GL061216

Clough, S. A., Shephard, M. W., Mlawer, E. J., Delamere, J. S., Iacono, M. J., Cady-Pereira, K., et al. (2005). Atmospheric radiative transfer modeling: A summary of the AER codes. *Journal of Quantitative Spectroscopy & Radiative Transfer*, *91*(2), 233–244. https://doi.org/10.1016/j.jqsrt.2004.05.058

Costa, S. M., & Shine, K. P. (2006). An estimate of the global impact of multiple scattering by clouds on outgoing long-wave radiation. *Quarterly Journal of the Royal Meteorological Society*, *132*(616), 885–895. https://doi.org/10.1256/qj.05.169.

Deng, M., Mace, G. G., Wang, Z., & Berry, E. (2015). CloudSat 2C-ICE product update with a new Ze parameterization in lidar-only region. *Journal of Geophysical Research: Atmospheres*, *120*, 12,198–12,208. https://doi.org/10.1002/2015JD023600

Deng, M., Mace, G. G., Wang, Z., & Okamoto, H. (2010). Tropical composition, cloud and climate coupling experiment validation for cirrus cloud profiling retrieval using CloudSat radar and CALIPSO lidar. *Journal of Geophysical Research*, *115*, D00J15. https://doi.org/10.1029/2009JD013104

Di Girolamo, L., Liang, L., & Platnick, S. (2010). A global view of one-dimensional solar radiative transfer through oceanic water clouds. *Geophysical Research Letters*, *37*, L18809. https://doi.org/10.1029/2010GL044094

van Diedenhoven, B., Fridlind, A. M., Cairns, B., Ackerman, A. S., & Yorks, J. (2016). Vertical variation of ice particle size in convective cloud tops. *Geophysical Research Letters*, *43*, 4586–4593. https://doi.org/10.1002/2016GL068548

Duncan, D. I., & Eriksson, P. (2018). An update on global atmospheric ice estimates from satellite observations and reanalyses. *Atmospheric Chemistry and Physics Discussions*, 1–20. https://doi.org/10.5194/acp-2018-275

Eliasson, S., Buehler, S. A., Milz, M., Eriksson, P., & John, V. O. (2011). Assessing observed and modelled spatial distributions of ice water path using satellite data. *Atmospheric Chemistry and Physics*, *11*(1), 375–391. https://doi.org/10.5194/acp-11-375-2011

Eriksson, P., Ekstrom, M., Rydberg, B., Wu, D. L., Austin, R. T., & Murtagh, D. P. (2008). Comparison between early Odin-SMR, Aura MLS and CloudSat retrievals of cloud ice mass in the upper tropical troposphere. *Atmospheric Chemistry and Physics*, *8*(7), 1937–1948. https://doi.org/10.5194/acp-8-1937-2008

Fauchez, T., Davis, A. B., Cornet, C., Szczap, F., Platnick, S., Dubuisson, P., & Thieuleux, F. (2017). A fast hybrid (3-D/1-D) model for thermal radiative transfer in cirrus via successive orders of scattering. *Journal of Geophysical Research: Atmospheres*, *122*, 344–366. https://doi.org/10.1002/2016JD025607

Fauchez, T., Dubuisson, P., Cornet, C., Szczap, F., Garnier, A., Pelon, J., & Meyer, K. (2015). Impacts of cloud heterogeneities on cirrus optical properties retrieved from space-based thermal infrared radiometry. *Atmospheric Measurement Techniques*, *8*(2), 633–647. https://doi.org/10.5194/amt-8-633-2015

Fauchez, T., Platnick, S., Meyer, K., Cornet, C., Szczap, F., & Várnai, T. (2017). Scale dependence of cirrus horizontal heterogeneity effects on TOA measurements—Part I: MODIS brightness temperatures in the thermal infrared. *Atmospheric Chemistry and Physics*, *17*(13), 8489–8508. https://doi.org/10.5194/acp-17-8489-2017

Fauchez, T., Platnick, S., Sourdeval, O., Wang, C., Meyer, K., Cornet, C., & Szczap, F. (2018). Cirrus horizontal heterogeneity and 3D radiative effects on cloud optical property retrievals from MODIS near to thermal infrared channels as a function of spatial resolution. *Journal of Geophysical Research: Atmospheres*, *123*, 11,141–11,153. https://doi.org/10.1029/2018JD028726

Feofilov, A. G., Stubenrauch, C. J., & Delanoë, J. (2015). Ice water content vertical profiles of high-level clouds: Classification and impact on radiative fluxes. *Atmospheric Chemistry and Physics*, *15*(21), 12,327–12,344. https://doi.org/10.5194/acp-15-12327-2015

Ferraro, R., Weng, F., Grody, N. C., Zhao, L., Meng, H., Kongoli, C., Pellegrino, P., et al. (2005). NOAA operational hydrological products derived from the Advanced Microwave Sounding Unit. *IEEE Transactions on Geoscience and Remote Sensing*, *43*(5), 1036–1049. https://doi.org/10.1109/TGRS.2004.843249

Fu, Q., & Liou, K. N. (1993). Parameterization of the radiative properties of cirrus clouds. *Journal of the Atmospheric Sciences*, *50*(13), 2008–2025. https://doi.org/10.1175/1520-0469(1993)050<2008:POTRPO>2.0.CO;2

Garnier, A., Pelon, J., Dubuisson, P., Faivre, M., Chomette, O., Pascal, N., & Kratz, D. P. (2012). Retrieval of cloud properties using CALIPSO imaging infrared radiometer. Part I: Effective emissivity and optical depth. *Journal of Applied Meteorology and Climatology*, *51*(7), 1407–1425. https://doi.org/10.1175/JAMC-D-11-0220.1

Garnier, A., Pelon, J., Dubuisson, P., Yang, P., Faivre, M., Chomette, O., et al. (2013). Retrieval of cloud properties using CALIPSO imaging infrared radiometer. Part I: Effective emissivity and optical depth. *Journal of Applied Meteorology and Climatology*, *52*(11), 2582–2599. https://doi.org/10.1175/JAMC-D-12-0328.1

Gelaro, R., McCarty, W., Suárez, M. J., Todling, R., Molod, A., Takacs, L., et al. (2017). The Modern-Era Retrospective Analysis for Research and Applications, Version 2 (MERRA-2). *Journal of Climate*, *30*(14), 5419–5454. https://doi.org/10.1175/JCLI-D-16-0758.1

Gong, J., & Wu, D. L. (2014). CloudSat-constrained cloud ice water path and cloud top height retrievals from MHS 157 and 183.3 GHz radiances. *Atmospheric Measurement Techniques*, *7*(6), 1873–1890. https://doi.org/10.5194/amt-7-1873-2014

Grosvenor, D. P., & Wood, R. (2014). The effect of solar zenith angle on MODIS cloud optical and microphysical retrievals within marine liquid water clouds. *Atmospheric Chemistry and Physics*, *14*(14), 7291–7321. https://doi.org/10.5194/acp-14-7291-2014

Ham, S. H., Sohn, B. J., Kato, S., & Satoh, M. (2013). Vertical structure of ice cloud layers from CloudSat and CALIPSO measurements and comparison to NICAM simulations. *Journal of Geophysical Research: Atmospheres*, *118*, 9930–9947. https://doi.org/10.1002/jgrd.50582

Heidinger, A. K., Foster, M. J., Walther, A., & Zhao, X. (2014). The pathfinder atmospheres extended (PATMOS-x) AVHRR climate data set. *Bulletin of the American Meteorological Society*, *95*(6), 909–922. https://doi.org/10.1175/BAMS-D-12-00246.1

Holl, G., Eliasson, S., Mendrok, J., & Buehler, S. A. (2014). SPARE-ICE: Synergistic ice water path from passive operational sensors. *Journal of Geophysical Research: Atmospheres*, *119*, 1504–1523. https://doi.org/10.1002/2013JD020759

Horváth, Á., & Davies, R. (2007). Comparison of microwave and optical cloud water path estimates from TMI, MODIS, and MISR. *Journal of Geophysical Research*, *112*, D01202. https://doi.org/10.1029/2006JD007101

Horváth, Á., Seethala, C., & Deneke, H. (2014). View angle dependence of MODIS liquid water path retrievals in warm oceanic clouds. *Journal of Geophysical Research: Atmospheres*, *119*, 8304–8328. https://doi.org/10.1002/2013JD021355

Houghton, J. T., Ding, Y., & Noguer, M. (2001). *Climate change 2001: The scientific basis* (p. 881). Cambridge, UK: Cambridge University Press.

Huang, X. L., Chen, X. H., Zhou, D. K., & Liu, X. (2016). An observationally based global band-by-band surface emissivity dataset for climate and weather simulations. *Journal of the Atmospheric Sciences*, *73*(9), 3541–3555. https://doi.org/10.1175/JAS-D-15-0355.1

Hubanks, P. A., Platnick, S., King, M. D., & Ridgway, B. (2016). MODIS atmosphere L3 gridded product Algorithm Theoretical Basis Document (ATBD) & Users Guide, Collection 006, Version 4.2., 2016. NASA-GSFC, 122. Retrieved from https://modis-images. gsfc.nasa.gov/_docs/L3_ATBD_C6.pdf (last access: 21 August 2017).

Iwabuchi, H., & Hayasaka, T. (2002). Effects of cloud horizontal inhomogeneity on the optical thickness retrieved from moderate-resolution satellite data. *Journal of the Atmospheric Sciences*, *59*(14), 2227–2242. https://doi.org/10.1175/1520-0469(2002)059<2227:EOCHIO>2.0.CO;2

Jiang, J. H., Su, H., Zhai, C., Perun, V. S., del Genio, A., Nazarenko, L. S., et al. (2012). Evaluation of cloud and water vapor simulations in CMIP5 climate models using NASA "A-Train" satellite observations. *Journal of Geophysical Research*, *117*, D14105. https://doi.org/10.1029/2011JD017237

Kahn, B. H., Schreier, M. M., Yue, Q., Fetzer, E. J., Irion, F. W., Platnick, S., et al. (2015). Pixel-scale assessment and uncertainty analysis of AIRS and MODIS ice cloud optical thickness and effective radius. *Journal of Geophysical Research: Atmospheres*, *120*, 11,669–11,689. https://doi.org/10.1002/2015JD023950

Khatri, P., Iwabuchi, H., & Saito, M. (2018). Vertical profiles of ice cloud microphysical properties and their impacts on cloud retrieval using thermal infrared measurements. *Journal of Geophysical Research: Atmospheres*, *123*, 5301–5319. https://doi.org/10.1029/2017JD028165

King, M. D., Platnick, S. E., Menzel, W. P., Ackerman, S. A., & Hubanks, P. A. (2013). Spatial and temporal distribution of clouds observed by MODIS onboard the Terra and Aqua satellites. *IEEE Transactions on Geoscience and Remote Sensing*, *51*(7), 3826–3852. https://doi.org/10.1109/TGRS.2012.2227333

Kuo, C. P., Yang, P., Huang, X. L., Feldman, D., Flanner, M., Kuo, C., & Mlawer, E. J. (2017). Impact of multiple scattering on longwave radiative transfer involving clouds. *Journal of Advances in Modeling Earth Systems*, *9*, 3082–3098. https://doi.org/10.1002/2017MS001117

Liang, L., Di Girolamo, L., & Sun, W. (2015). Bias in MODIS cloud drop effective radius for oceanic water clouds as deduced from optical thickness variability across scattering angles. *Journal of Geophysical Research: Atmospheres*, *120*, 7661–7681. https://doi.org/10.1002/2015JD023256

Mace, G. G., & Zhang, Q. (2014). The CloudSat radar-lidar geometrical profile product (RL-GeoProf): Updates, improvements, and selected results. *Journal of Geophysical Research: Atmospheres*, *119*, 9441–9462. https://doi.org/10.1002/2013JD021374

Marshak, A., Platnick, S., Várnai, T., Wen, G., & Cahalan, R. F. (2006). Impact of three-dimensional radiative effects on satellite retrievals of cloud droplet sizes. *Journal of Geophysical Research*, *111*, D09207. https://doi.org/10.1029/2005JD006686

McClatchey, R. A., Fenn, R. W., Salby, J. E. A., Volz, F. E., and Garing, J. S. (1972), Optical properties of the atmosphere. Air Force Cambridge Res. Lab. Tech. Rep. AFCRL-72-0497 (108 pp.).

Meyer, K., Platnick, S., Arnold, G. T., Holz, R. E., Veglio, P., Yorks, J., & Wang, C. (2016). Cirrus cloud optical and microphysical property retrievals from eMAS during SEAC4RS using bi-spectral reflectance measurements within the 1.88 μm water vapor absorption band. *Atmospheric Measurement Techniques*, *9*(4), 1743–1753. https://doi.org/10.5194/amt-9-1743-2016

Miller, D. J., Zhang, Z., Ackerman, A. S., Platnick, S., & Baum, B. A. (2016). The impact of cloud vertical profile on liquid water path retrieval based on the bi-spectral method: A theoretical study based on large-eddy simulations of shallow marine boundary-layer clouds. *Journal of Geophysical Research: Atmospheres*, *121*, 4122–4141. https://doi.org/10.1002/2015JD024322

Miller, S. D., Noh, Y.-J., & Heidinger, A. K. (2014). Liquid-top mixed-phase cloud detection from shortwave-infrared satellite radiometer observations: A physical basis. *Journal of Geophysical Research: Atmospheres*, *119*, 8245–8267. https://doi.org/10.1002/2013JD021262

Minnis, P., Sun-Mack, S., Young, D. F., Heck, P. W., Garber, D. P., Chen, Y., et al. (2011). CERES edition-2 cloud property retrievals using TRMM VIRS and Terra and Aqua MODIS data—Part I: Algorithms. *IEEE Transactions on Geoscience and Remote Sensing*, *49*(11), 4374–4400. https://doi.org/10.1109/TGRS.2011.2144601

Morrison, H., & Mibrandt, J. A. (2015). Parameterization of cloud microphysics based on the prediction of bulk ice particle properties. Part I: Scheme description and idealized tests. *Journal of the Atmospheric Sciences*, *72*(1), 287–311. https://doi.org/10.1175/JAS-D-14-0065.1

Mülmenstädt, J., Sourdeval, O., Delanoë, J., & Quaas, J. (2015). Frequency of occurrence of rain from liquid-, mixed-, and ice-phase clouds derived from A-Train satellite retrievals. *Geophysical Research Letters*, *42*, 6502–6509. https://doi.org/10.1002/2015GL064604

Nakajima, T., & King, M. D. (1990). Determination of the optical thickness and effective particle radius of clouds from reflected solar radiance measurements. Part I: Theory. *Journal of the Atmospheric Sciences*, *47*(15), 1878–1893. https://doi.org/10.1175/1520-0469(1990)047<1878:DOTOTA>2.0.CO;2

Otkin, J. A., & Greenwald, T. J. (2008). Comparison of WRF model-simulated and MODIS-derived cloud data. *Monthly Weather Review*, *136*(6), 1957–1970. https://doi.org/10.1175/2007MWR2293.1

Platnick, S. (2000). Vertical photon transport in cloud remote sensing problems. *Journal of Geophysical Research*, *105*(D18), 22,919–22,935. https://doi.org/10.1029/2000JD900333

Platnick, S., Meyer, K. G., King, M. D., Wind, G., Amarasinghe, N., Marchant, B., et al. (2017). The MODIS cloud optical and microphysical products: Collection 6 updates and examples from Terra and Aqua. *IEEE Transactions on Geoscience and Remote Sensing*, *55*(1), 502–525. https://doi.org/10.1109/TGRS.2016.2610522

Platnick, S., & Valero, F. P. (1995). A validation of a satellite cloud retrieval during ASTEX. *Journal of the Atmospheric Sciences*, *52*(16), 2985–3001. https://doi.org/10.1175/1520-0469(1995)052<2985:AVOASC>2.0.CO;2

Randall, D. A., Wood, R. A., Bony, S., Colman, R., Fichefet, T., Fyfe, J., et al. (2007). Cilmate Models and Their Evaluation. In S. Solomon et al. (Eds.), *Climate Change 2007: The Physical Science Basis. Contribution of Working Group I to the Fourth Assessment Report of the Intergovernmental Panel on Climate Change.* Cambridge, United Kingdom and New York: Cambridge University Press.

Rodgers, C. D. (2000). *Inverse Methods for Atmospheric Sounding, Theory and Practice* (73 pp.). Hackensack, NJ: World Scientific.

Roebeling, R. A., Feijt, A. J., & Stammes, P. (2006). Cloud property retrievals for climate monitoring: Implications of differences between Spinning Enhanced Visible and Infrared Imager (SEVIRI) on METEOSAT-8 and Advanced Very High Resolution Radiometer (AVHRR) on NOAA-17. *Journal of Geophysical Research*, *111*, D20210. https://doi.org/10.1029/2005JD006990

Rossow, W. B., & Schiffer, R. A. (1999). Advances in understanding clouds from ISCCP. *Bulletin of the American Meteorological Society*, *80*(11), 2261–2287. https://doi.org/10.1175/1520-0477(1999)080<2261:AIUCFI>2.0.CO;2

Schmitt, C. G., & Heymsfield, A. J. (2010). The dimensional characteristics of ice crystal aggregates from fractal geometry. *Journal of the Atmospheric Sciences*, *67*(5), 1605–1616. https://doi.org/10.1175/2009JAS3187.1

Seethala, C., & Horváth, Á. (2010). Global assessment of AMSR-E and MODIS cloud liquid water path retrievals in warm oceanic clouds. *Journal of Geophysical Research*, *115*, D13202. https://doi.org/10.1029/2009JD012662

Sourdeval, O., Labonnote, L. C., Brogniez, G., Jourdan, O., Pelon, J., & Garnier, A. (2013). A variational approach for retrieving ice cloud properties from infrared measurements: Application in the context of two IIR validation campaigns. *Atmospheric Chemistry and Physics*, *13*(16), 8229–8244. https://doi.org/10.5194/acp-13-8229-2013

Stamnes, K., Tsay, S.-C., Wiscombe, W., & Jayaweera, K. (1988). Numerically stable algorithm for discrete-ordinate-method radiative transfer in multiple scattering and emitting layered media. *Applied Optics*, *27*(12), 2502–2509. https://doi.org/10.1364/AO.27.002502

Stephens, G. L., & Kummerow, C. D. (2007). The remote sensing of clouds and precipitation from space: A review. *Journal of the Atmospheric Sciences*, *64*(11), 3742–3765. https://doi.org/10.1175/2006JAS2375.1

Stephens, G. L., Li, J., Wild, M., Clayson, C. A., Loeb, N., Kato, S., L'Ecuyer, T., et al. (2012). An update on Earth's energy balance in light of the latest global observations. *Nature Geoscience*, *5*(10), 691–696. https://doi.org/10.1038/ngeo1580

Stephens, G. L., Vane, D. G., Boain, R. J., Mace, G. G., Sassen, K., Wang, Z., et al., & the CloudSat Science Team (2002). The CloudSat mission and the A-Train: A new dimension of space-based observations of clouds and precipitation. *Bulletin of the American Meteorological Society*, *83*(12), 1771–1790. https://doi.org/10.1175/BAMS-83-12-1771

Stubenrauch, C. J., Rossow, W. B., Kinne, S., Ackerman, S., Cesana, G., Chepfer, H., et al. (2013). Assessment of global cloud datasets from satellites: Project and database initiated by GEWEX radiation panel. *Bulletin of the American Meteorological Society*, *94*(7), 1031–1049. https://doi.org/10.1175/BAMS-D-12-00117.1

Su, H., Jiang, J. H., Zhai, C., Perun, V., Shen, J. T., Del Genio, A. D., et al. (2013). Diagnosis of regime-dependent cloud simulation errors in CMIP5 models using "A-Train" satellite observations and reanalysis data. *Journal of Geophysical Research: Atmospheres*, *118*, 2762–2780. https://doi.org/10.1029/2012JD018575

Taylor, K. E., Stouffer, R. J., & Meehl, G. A. (2012). An overview of CMIP5 and the experiment design. *Bulletin of the American Meteorological Society*, *93*(4), 485–498. https://doi.org/10.1175/BAMS-D-11-00094.1

Trenberth, K. E., Fasullo, J. T., & Kiehl, J. (2009). Earth's global energy budget. *Bulletin of the American Meteorological Society*, *90*(3), 311–324. https://doi.org/10.1175/2008BAMS2634.1

Twomey, S., & Cocks, T. (1989). Remote sensing of cloud parameters from spectral reflectance in the near-infrared. *Beitr. Phys. Atmos*, *62*, 172–179.

Várnai, T., & Davies, R. (1999). Effects of cloud heterogeneities on shortwave radiation: Comparison of cloud-top variability and internal heterogeneity. *Journal of the Atmospheric Sciences*, *56*(24), 4206–4224. https://doi.org/10.1175/1520-0469(1999)056<4206:EOCHOS>2.0.CO;2

Vogelmann, A. M., & Ackerman, T. P. (1995). Relating cirrus cloud properties to observed fluxes: A critical assessment. *Journal of the Atmospheric Sciences*, *52*(23), 4285–4301. https://doi.org/10.1175/1520-0469(1995)052<4285:RCCPTO>2.0.CO;2

Waliser, D. E., Seo, K. W., Schubert, S., & Njoku, E. (2007). Global water cycle agreement in IPCC AR4 model simulations. *Geophysical Research Letters*, *34*, L16705. https://doi.org/10.1029/2007GL030675

Waliser, D. E., Li, J.-L. F., Woods, C. P., Austin, R. T., Bacmeister, J., Chern, J., et al. (2009). Cloud ice: A climate model challenge with signs and expectations of progress. *Journal of Geophysical Research*, *114*, D00A21. https://doi.org/10.1029/2008JD010015

Wang, C., Platnick, S., Zhang, Z., Meyer, K., Wind, G., & Yang, P. (2016). Retrieval of ice cloud properties using an optimal estimation algorithm and MODIS infrared observations. Part II: Retrieval evaluation. *Journal of Geophysical Research: Atmospheres*, *121*, 5827–5845. https://doi.org/10.1002/2015JD024528

Wang, C., Platnick, S., Zhang, Z., Meyer, K., & Yang, P. (2016). Retrieval of ice cloud properties using an optimal estimation algorithm and MODIS infrared observations. Part I: Forward model, error analysis, and information content. *Journal of Geophysical Research: Atmospheres*, *121*, 5809–5826. https://doi.org/10.1002/2015JD024526

Wang, C., Yang, P., Baum, A. B., Platnick, S., Heidinger, A. K., Hu, Y. X., & Holz, R. E. (2011). Retrieval of ice cloud optical thickness and effective particle size using a fast infrared radiative transfer model. *Journal of Applied Meteorology and Climatology*, *50*(11), 2283–2297. https://doi.org/10.1175/JAMC-D-11-067.1

Wang, J., Liu, C., Min, M., Hu, X., & Husi, L. (2018). Effects and applications of satellite radiometer 2.25-μm channel on cloud property retrievals. *IEEE Transactions on Geoscience and Remote Sensing*, *56*(9), 5207–5216. https://doi.org/10.1109/TGRS.2018.2812082

Winker, D. M., Tackett, J. L., Getzewich, B. J., Liu, Z., Vaughan, M. A., & Rogers, R. R. (2013). The global 3-D distribution of tropospheric aerosols as characterized by CALIOP. *Atmospheric Chemistry and Physics*, *13*(6), 3345–3361. https://doi.org/10.5194/acp-13-3345-2013

Wood, R., & Hartmann, D. L. (2006). Spatial variability of liquid water path in marine low cloud: The importance of mesoscale cellular convection. *Journal of Climate*, *19*(9), 1748–1764. https://doi.org/10.1175/JCLI3702.1

Wu, D. L., Austin, R. T., Deng, M., Durden, S. L., Heymsfield, A. J., Jiang, J. H., et al. (2009). Comparisons of global cloud ice from MLS, CloudSat, and correlative data sets. *Journal of Geophysical Research*, *114*, D00A24. https://doi.org/10.1029/2008JD009946

Yang, P., Bi, L., Baum, B. A., Liou, K., Kattawar, G. W., Mishchenko, M. I., & Cole, B. (2013). Spectrally consistent scattering, absorption, and polarization properties of atmospheric ice crystals at wavelengths from 0.2 to 100 μm. *Journal of the Atmospheric Sciences*, *70*(1), 330–347. https://doi.org/10.1175/JAS-D-12-039.1

Yang, P., Zhang, L., Hong, G., Nasiri, S. L., Baum, B. A., Huang, H.-L., et al. (2007). Differences between collection 4 and 5 MODIS ice cloud optical/microphysical products and their impact on radiative forcing simulations. *IEEE Transactions on Geoscience and Remote Sensing*, *45*(9), 2886–2899. https://doi.org/10.1109/TGRS.2007.898276

Yang, Y., & Di Girolamo, L. (2008). Impacts of 3-D radiative effects on satellite cloud detection and their consequences on cloud fraction and aerosol optical depth retrievals. *Journal of Geophysical Research*, *113*, D04213. https://doi.org/10.1029/2007JD009095

Yi, B., Rapp, A. D., Yang, P., Baum, B. A., & King, M. D. (2017). A comparison of Aqua MODIS ice and liquid water cloud physical and optical properties between collection 6 and collection 5.1: Pixel-to-pixel comparisons. *Journal of Geophysical Research: Atmospheres*, *122*, 4528–4549. https://doi.org/10.1002/2016JD025586

Zhang, D., Wang, Z., & Liu, D. (2010). A global view of midlevel liquid-layer topped stratiform cloud distribution and phase partition from CALIPSO and CloudSat measurements. *Journal of Geophysical Research*, *115*, D00H13. https://doi.org/10.1029/2009JD012143

Zhang, Z., Ackerman, A. S., Feingold, G., Platnick, S., Pincus, R., & Xue, H. (2012). Effects of cloud horizontal inhomogeneity and drizzle on remote sensing of cloud droplet effective radius: Case studies based on large-eddy simulations. *Journal of Geophysical Research*, *117*, D19208. https://doi.org/10.1029/2012JD017655

Zhang, Z., Platnick, S., Yang, P., Heidinger, A. K., & Comstock, J. M. (2010). Effects of ice particle size vertical inhomogeneity on the passive remote sensing of ice clouds. *Journal of Geophysical Research*, *115*, D17203. https://doi.org/10.1029/2010JD013835

Zhang, Z., Werner, F., Cho, H.-M., Wind, G., Platnick, S., Ackerman, A. S., Di Girolamo, L., et al. (2016). A framework based on 2-D Taylor expansion for quantifying the impacts of subpixel reflectance variance and covariance on cloud optical thickness and effective radius retrievals based on the bispectral method. *Journal of Geophysical Research: Atmospheres*, *121*, 7007–7025. https://doi.org/10.1002/2016JD024837

Zhang, Z., Yang, P., Kattawar, G., Riedi, J., C.-Labonnote, L., Baum, B. A., et al. (2009). Influence of ice particle model on satellite ice cloud retrieval: Lesion learned from MODIS and POLDER cloud product comparison. *Atmospheric Chemistry and Physics*, *9*(18), 7115–7129. https://doi.org/10.5194/acp-9-7115-2009

Zhou, C., Zelinka, M. D., Dessler, A. E., & Yang, P. (2013). An analysis of the short-term cloud feedback using MODIS data. *26*(13), 4803–4815. https://doi.org/10.1175/JCLI-D-12-00547.1